

Tectonics

RESEARCH ARTICLE

10.1029/2018TC005459

Key Points:

- We investigated active faults in the western Ili Basin in the Tien Shan by remote sensing, field studies, earthquake seismology, and GPS data
- Large left-lateral strike-slip faults accommodate a NE-SW shear component
- Oblique right-lateral faults transfer deformation between large left-lateral strike-slip faults and accommodate shortening by rotation about vertical axes

Supporting Information:

- Supporting Information S1

Correspondence to:

C. Grützner,
christoph.gruetzner@uni-jena.de

Citation:

Grützner, C., Campbell, G., Walker, R. T., Jackson, J., Mackenzie, D., Abdrakhmatov, K., & Mukambayev, A. (2019). Shortening accommodated by thrust and strike-slip faults in the Ili Basin, northern Tien Shan. *Tectonics*, 38, 2255–2274. <https://doi.org/10.1029/2018TC005459>


Received 19 DEC 2018

Accepted 30 MAY 2019

Accepted article online 7 JUN 2019

Published online 5 JUL 2019

Shortening Accommodated by Thrust and Strike-Slip Faults in the Ili Basin, Northern Tien Shan

C. Grützner^{1,2} , G. Campbell^{1,3}, R.T. Walker⁴, J. Jackson¹, D. Mackenzie⁴, K. Abdrakhmatov⁵, and A. Mukambayev⁶

¹COMET, Bullard Labs, Department of Earth Sciences, University of Cambridge, Cambridge, UK, ²Now at Institute of Geological Sciences, Friedrich Schiller University Jena, Jena, Germany, ³Now at ARUP, London, UK, ⁴Department of Earth Sciences, University of Oxford, Oxford, UK, ⁵Kyrgyz Seismological Institute, Academy of Sciences of the Kyrgyz Republic, Bishkek, Kyrgyz Republic, ⁶Kazakhstan National Data Center, Almaty, Kazakhstan

Abstract The Tien Shan accommodates a significant portion of the India-Eurasia N-S convergence. In its northern part a zigzag pattern of mountain ranges bounds the western Ili Basin. The role of this basin in the overall shortening and the regional kinematics is not well understood. Geodetic data and instrumental seismicity are not sufficient to infer the role of individual faults and fault systems. We analyze GPS data and earthquake slip vectors and present the results of fault mapping based on remote sensing and field campaigns in the western Ili Basin. These observations indicate that E-W thrust faults are active at the basin margins, and oblique and strike-slip faults, both in the basin and in the Paleozoic rocks within the mountain ranges, have been active in the Late Quaternary. We propose a regional tectonic model in which the left-lateral strike-slip faults at the NW margin of the basin accommodate ~3-mm/year NE-SW shear. Smaller right-lateral oblique faults transfer the motion in between the left-lateral faults, and also take up shortening by rotations about vertical axes. We see the onset of internal deformation within the Ili Basin, although it has a strong basement. Our kinematic model is consistent with geodetic data, earthquake seismology, historical, and prehistorical surface faulting, and describes the first-order features of active deformation that can be observed in the northern Tien Shan. Our study illustrates the importance of combining these different data sets to understand the regional tectonics.

1. Introduction

Nearly half of the convergent motion between India and Eurasia is accommodated within the Tien Shan, more than 1,000 km north of the edge of stable India (Abdrakhmatov et al., 1996). This growing mountain range has seen some of the largest intracontinental earthquakes documented in the past 150 years (e.g., Krüger et al., 2015; Kulikova & Krüger, 2015; Molnar & Deng, 1984) and major faults with lengths of up to several hundred kilometers stand out in the geomorphology features (Avouac et al., 1993; Avouac & Tapponnier, 1993; Campbell et al., 2015). The Tien Shan hosts a large number of E-W and NE-SW elongated ranges, which are separated by intramontane and intermontane basins (Figure 1). The basins are especially large in the central and eastern Tien Shan. The Tarim Basin and the Dzhungar Basin (also referred to as Junggar Basin) bound the Tien Shan to the south and the Borohoro Shan to the northeast, respectively. They are commonly interpreted as former microcontinents and behave more or less as rigid blocks in the overall compressive regime, showing little internal deformation but localized shortening at their margins (Allen et al., 1991, 1993; Allen et al., 1999; Allen & Vincent, 1997; Buckman & Aitchison, 2004; Carroll et al., 1995; Sobel & Dumitru, 1997; Thompson Jobe et al., 2017; Zhang et al., 1984). Although the Tarim Basin has some internal deformation structures such as the Mazar Tagh Fault System (Pan et al., 2010), most of the shortening is accommodated at or near the southern front of the Tien Shan and the northeastern front of the Pamir (Bufe et al., 2017; Thompson Jobe et al., 2017, 2018). Intramontane basins in the Tien Shan such as the Bayanbulak Basin (e.g., Charreau et al., 2017; Jolivet et al., 2010) and the Naryn Basin (e.g., Burbank et al., 1999; Goode et al., 2011) are E-W elongated. They are overthrust by bedrock along their margins and also deform internally on structures that parallel the surrounding mountain ranges (Thompson et al., 2002).

The Ili Basin (also referred to as Yili) is an E-W elongated, triangular block between the northern Tien Shan and the Dzhungarian Alatau that opens toward the Kazakh Platform (Figure 1). This basin is located in a zone of compression and left-lateral shear. Although the Ili block is also an accreted sliver of continental

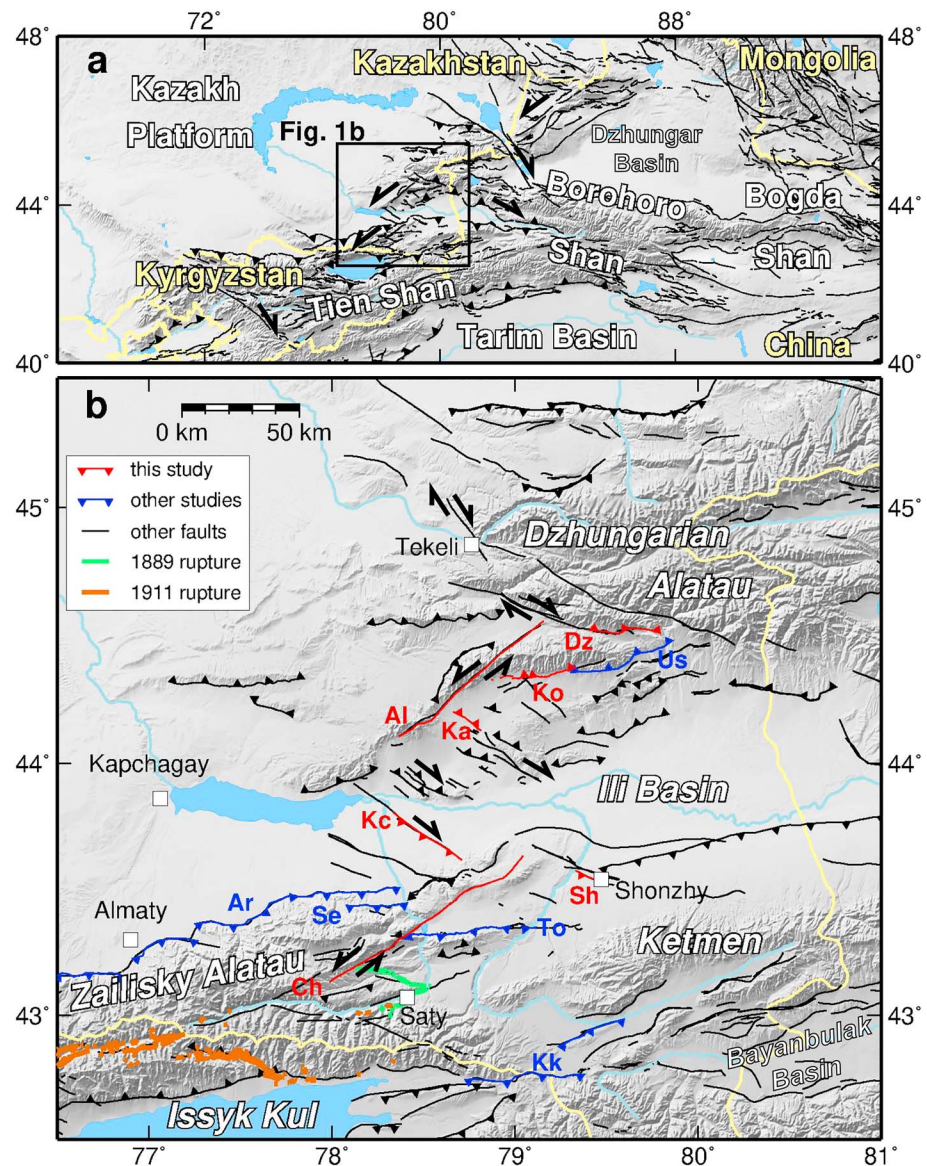


Figure 1. (a) Location of the Tien Shan range in central Asia. The extent of Figure 1b is outlined. Hillshade based on Etopo1 data. Mercator projection. (b) The Ili Basin region. Active faults mapped remotely and in the field are black. Red lines mark faults discussed here in detail: Al = Altyn Emel Fault, Ch = Chilik-Chon-Kemin Fault zone, Dz = Southern Dzhungarian Range Front Fault, Ka = Kalinino Fault, Kc = Fault near Kapchagay reservoir, Ko = Konyrolen Fault, Sh = Shonzhay Fault. Blue lines are active faults discussed in previous studies: Ar = Almaty Range Front Fault (Grützner, Walker, et al., 2017), Kk = Karkara Faults (Mackenzie et al., 2018), Se = Almaty Range Front Fault (Selander et al., 2012), To = Toraigyr Fault (Grützner, Carson, et al., 2017), Us = Uzek Thrust (Cording et al., 2014). The surface ruptures of the 1889 Chilik earthquake are marked in green (Abdrakhmatov et al., 2016); brown lines are those of the 1911 Chon Kemin earthquake (Arrowsmith et al., 2017). Hillshade based on SRTM3 data. Mercator projection.

crust that was either part of the Kazakhstan-Ili plate or a separate microcontinent in the Paleozoic (Charvet et al., 2011; Gao et al., 2009; Heubeck, 2001; Zhang et al., 1984), the narrow eastern part of the basin resembles the deformational style of the intramontane basins elsewhere in the Tien Shan with approximately E-W striking thrust faults paralleling the mountain fronts. Its western part, though, is very different. It is bounded by major E-W thrust faults to the north and to the south, and by a NE-SW left-lateral strike-slip zone in the west (Figure 1a). Close to the western basin margin, a number of smaller faults with a NW-SE trend are also observed (Figure 1b; e.g., Cording et al., 2014; Kober et al., 2013). So far little is known about the active tectonics of the western Ili Basin and what role it plays in

accommodating shortening and shear. It is also not fully understood whether its Paleozoic history as a block of rather rigid continental crust leads to a deformation style similar to that of Tarim and Dzhungar, or instead resembles a closing intramontane basin such as Naryn or Bayanbulak.

In order to understand how the regional deformation affects, and is related to, the Ili Basin, we analyzed all evidence of active faulting that we were able to identify in the study area (Figure 1b). Kompsat satellite imagery with 1-m resolution was used to visually evaluate evidence for active faulting. We used digital elevation models (DEMs) from SRTM1 and ALOS JAXA 30-m data, and the High Mountain Asia 8-m DEM (HMA; Shean, 2017) to detect morphological evidence for recent tectonic activity. Aerial imagery was collected from helikite and drone surveys, which allowed construction of high-resolution DEMs using the Structure-from-Motion technique (SfM; Grützner, Carson, et al., 2017; Grützner, Walker, et al., 2017; Johnson et al., 2014; Westoby et al., 2012). Several field campaigns were conducted during which we mapped faults and measured offset markers with differential GPS (DGPS). To supplement the geomorphological work, we analyzed GPS and earthquake data available from previous studies, and we determined slip vectors, focal mechanisms, and depths for other additional earthquakes.

2. Tectonic Background

The Proterozoic basement of the Tien Shan consists of a series of amalgamated microcontinents and island arcs that accreted mainly during the late Paleozoic (Allen et al., 1993; Heubeck, 2001; Şengör et al., 1993; Zhang et al., 1984). The Ili block, either an independent microcontinent or part of a larger continental block, collided with northern Tarim to the south and the North Tien Shan magmatic arc to the north after an episode of Carboniferous-Permian rifting (Pirajno et al., 2008). In the Late Permian, left-lateral shear and counterclockwise rotations of blocks led to a configuration close to present-day general structure of the Tien Shan (Allen et al., 1995). In the early Mesozoic, an episode of uplift affected the Ili block and its surroundings, probably caused by the far-field effect of collisions further south (Allen et al., 1991; Dewey et al., 1988; Molnar et al., 1987). During this phase of mountain building, N-S contraction prevailed throughout the region. Increased sediment input in the Jurassic was probably caused by a combination of thermal subsidence and downward flexure of foreland basins under the load of the growing mountain ranges (Allen et al., 1991). Tectonic quiescence prevailed in the Tien Shan from the Mesozoic until the early Cenozoic and led to erosion and peneplanation of the mountain ranges (Burbank et al., 1999; Goryachev, 1959; Makarov, 1977). The uplift of the Tien Shan as a result of the India-Eurasia collision started before the Neogene in some parts of the range. In the northern Tien Shan, uplift has prevailed since at least the late Miocene (Bullen et al., 2003; Sobel et al., 2006) on approximately E-W trending reverse faults.

Four stages of neotectonic activity are usually distinguished in the northern Tien Shan and the Ili Basin based on sediment analyses and thermochronology (Burtman, 2012; Han et al., 2004). Uplift at the northern margin started in the late Eocene-Oligocene (Hellwig et al., 2018) and led to depocenters in the northern part of the Ili Basin, while there is little evidence for sedimentation in the south. Alluvial fans formed at the basin margins and distal, fine-grained units were deposited in the central part of the basin (Kober et al., 2013). In the Miocene, both the northern and southern marginal faults have become active. This initiation of the main tectonic uplift is also evident from thermochronological data from the northern Tien Shan (Hendrix et al., 1994). In the western Ili Basin, arid conditions prevailed and basin closure is recorded in the middle-late Miocene (Verestek et al., 2018). Evaporitic layers that formed in continental mudflat conditions alternate with coarse flood deposits in the central Ili Basin (Frisch et al., 2019; Voigt et al., 2017). Middle to late Miocene variations in the sedimentary system of the Ili Basin, however, point to a phase of little tectonic activity only (Frisch et al., 2019). The third stage is a late Pliocene-early Pleistocene peak of tectonic activity with significant uplift on the E-W thrust faults and N-S basin shortening. The sediment record from that period includes coarse clastics that unconformably overlay the Miocene strata. A folded, 1,700-m-thick succession of fine-grained distal Neogene sediments from the Aktau Hills in the northwestern Ili Basin testifies to significant shortening (Voigt et al., 2017). Finally, N-S shortening in the eastern Ili Basin continues since middle Pleistocene but with lower rates (Han et al., 2004). Folded Pleistocene alluvial material disconformably overlies the Neogene Aktau units and shows that internal deformation affects the northern half of the Ili Basin. Today, rivers that drain the mountain ranges to the north and to the south of the Ili Basin such as the

Charyn River incise deeply into the older Cenozoic sequences, testifying to erosion related to the ongoing growth of the Tien Shan.

2.1. Field Studies of Active Faulting

Only a few studies have so far investigated field evidence for past surface-faulting earthquakes in the study area (Figure 1b). The 1889 Chilik earthquake ruptured an ~175-km-long, zigzag-shaped set of oblique thrust faults in the south of the Ili Basin area (green line in Figure 1b; Abdrakhmatov et al., 2016). A NE-SW striking, left-lateral surface rupture was observed in the Saty Valley (Figure 1b). Another set of WNW trending set of ruptures extends from the Saty valley to the north, and connects this zone to the large NE-SW striking Chilik-Chon-Kemin Fault system (Ch in Figure 1b), which likely ruptured during the 1911 Chon Kemin earthquake in its south-westernmost part (Arrowsmith et al., 2017; brown line in Figure 1b).

Kober et al. (2013) investigated thrust-related basement uplifts in the Ili Basin. Mapping of active faults and anticlines led them to conclude that thick-skinned thrusting along steeply dipping faults dominates the region today. They found that NW striking basement faults played a major role during the Cenozoic deformation phase in some parts of their study area. The NE to E strike of the major mountain ranges does not follow the trend of inherited structures from earlier tectonic events, suggesting that reactivation may influence, but not dominate, strain localization today (Kober et al., 2013).

Selander et al. (2012) investigated large-scale tectonic structures in the Kungey and Zailisky ranges north of Lake Issyk Kul. They discuss the role of large inherited strike-slip faults for the nucleation of thrust faults in the mountain ranges and propose a mega-flower structure that exerts control on present-day basement-cored uplifts. Cording et al. (2014) studied deformed river terraces at the southern mountain front of the Dzhungarian Alatau in the north of the Ili Basin. Using ^{10}Be exposure dating on the Usek Thrust they measured vertical and horizontal slip rates of ~0.4 and ~0.25 mm/year, respectively.

Grützner, Carson, et al. (2017) studied the Toraigyr Fault in the south of the Ili Basin (To in Figure 1b). Using remote sensing, DGPS, field studies, and paleoseismological trenching they conclude on two surface-rupturing earthquakes in the last ~40 ka. Along the Almaty Range Front, Selander et al. (2012) and Grützner, Walker, et al. (2017) document geomorphological evidence for recent active faulting. However, none of these studies dealt with the overall kinematics of active faulting across the Ili Basin.

Mackenzie et al. (2018) found that the Karkara Range front Fault (Kk in Figure 1b) creeps at a rate of 3.1–5.2 mm/year and that a fold in the Kegen basin deforms with at least 0.8 mm/year. They conclude that the overall horizontal shortening across this range front is at least 1.1–3.3 mm/year.

2.2. Constraints on Crustal Deformation From GPS

N-S shortening rates in the Tien Shan decrease from west to east (Abdrakhmatov et al., 1996; Zubovich et al., 2010) caused by a clockwise rotation of the rigid Tarim Basin with respect to the stable Kazakh Platform (Avouac et al., 1993; Avouac & Tapponnier, 1993). At the longitude of our study area, around 12–15 mm/year of shortening is seen in GPS data, of which ~5 mm/year is accommodated across the southern margin of the Tien Shan (Zubovich et al., 2010; Figure 2). In our study area, the Tien Shan and the Dzhungarian Alatau are characterized by large NE-SW trending mountains (Altyn Emel and Chilik-Kemin) that connect the predominant E-W trending ranges (Zailisky Alatau, Dzhungarian Alatau, and Ketmen ranges; Figure 1b). The Ili Basin is bordered by these ranges and opens to the Kazakh Platform in the west. GPS data (Zubovich et al., 2010) reveal a distinct change in GPS velocities and directions relative to Eurasia. We projected the GPS velocities onto a N-S transect across the basin and included all stations within 0.5° on either side of this line. We found that 3–5 mm/year of N-S shortening is accommodated uniformly across the Ili Basin and its margins, rather than being localized on any one structure (Figures 2a and 2b). South of the Dzhungarian Alatau the GPS velocities with respect to the stable Kazakh platform (i.e., Eurasia) have a NNE trend. They change toward NNW-NW directions north and northwest of the Ili Basin. Along the S-N transect, the E-W velocities change from ~1 mm/year eastward to ~1-mm/year westward motion (Figure 2b), indicating a zone of range-parallel left-lateral shear.

A second transect that strikes perpendicular to the NE-SW trending mountain ranges illustrates the change of GPS velocities at the western basin margin. We projected the GPS data from 0.5° on either side of the

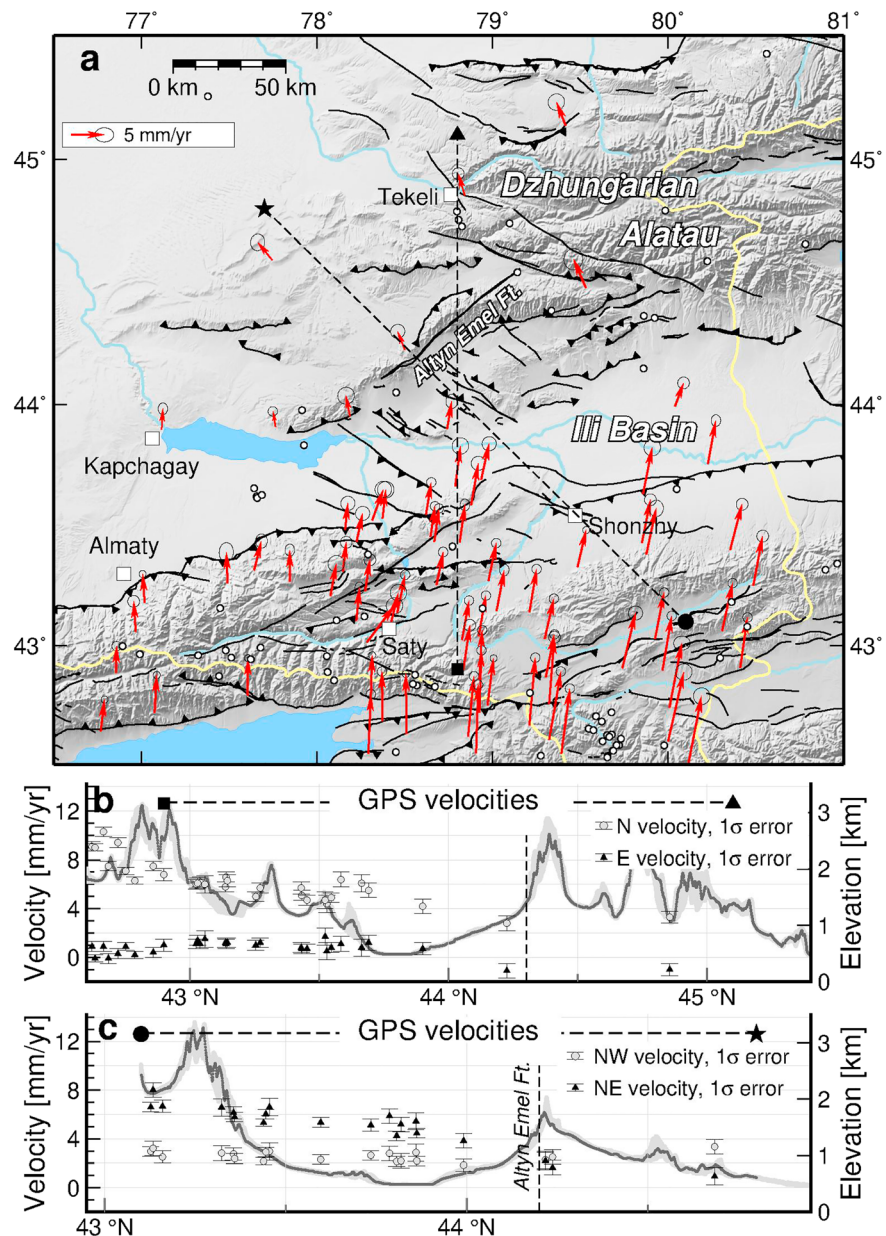


Figure 2. (a) GPS velocities relative to Eurasia with 95% confidence ellipses are from Zubovich et al. (2010). White dots are earthquakes $> m_b 4.5$ 1960–2008 from the catalogues of Engdahl et al. (1998) and ISC from 2009 to 2018 (ISC, 2018). The dashed black lines mark transects which the GPS velocities are projected onto in Figures 2b and 2c. (b) East and north GPS velocities projected onto the dashed line with square and triangle end points in Figure 2a using all stations within 0.5° either side of the line with their standard errors. Dark grey line is the 0.05° smoothed SRTM3 topography along the profile line plotted above a 0.02° -wide topography swath in light grey. (c) Northwest and northeast GPS velocity components for the profile marked with the circle and star end points in Figure 2a. Note the drop in NE velocities around the latitude of the Altyn Emel Fault, which indicates left-lateral shear.

profile onto the profile line and calculated the velocity components parallel and perpendicular to the strike, respectively (Figure 2c). The NW components of motion relative to Eurasia are almost constant within error bars along the transect. The NE velocities drop from 6 to 8 mm/year at the SE end of the profile to 1–2 mm/year at the NW end. A pronounced decline in NE velocities is observed at around 44°N , where the NE-SW striking Altyn Emel range bounds the basin. This indicates significant left-lateral shear at the basin margin. Around 6 mm/year of left-lateral shear is accommodated across the entire study area, of which ~ 3 mm/year are taken up at the NW margin of the Ili Basin.

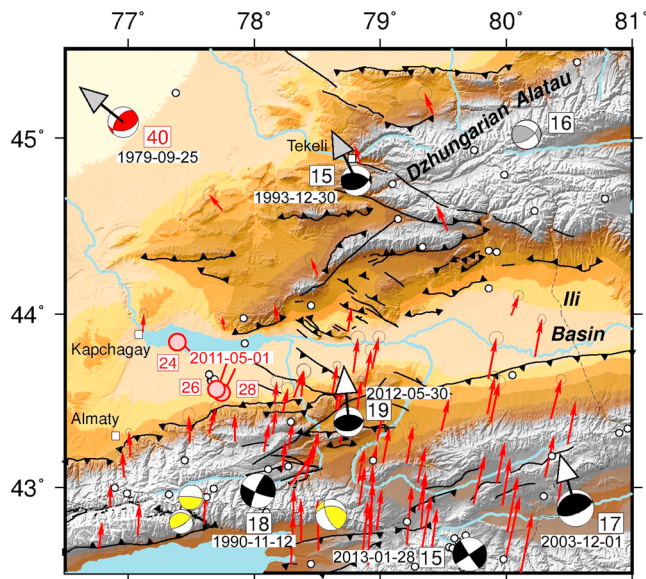


Figure 3. GPS velocities relative to Eurasia with 95% confidence ellipses from Zubovich et al. (2010), with the same scale as in Figure 2. White dots are earthquakes $> m_b 4.5$ 1960–2008 from the catalogues of Engdahl et al. (1998) and ISC from 2009 to 2018 (ISC, 2018). Well-constrained fault plane solutions from teleseismic body wave form inversion are from Sloan et al. (2011) and events modeled in this study. Red > 20 km, black < 20 -km depth. Additional fault plane solutions are from CMTs (yellow, with no independent depth control). Pink circles indicate three earthquakes with magnitudes between $M_{4.7}$ and $M_{5.3}$, for which depths were confirmed by array-waveform modeling by Craig et al. (2012). Numbers in white rectangles are well-constrained depths and dates. Large arrows indicate slip vector azimuths, south side relative to north. For the two thrust events in the south (white arrows) the rake is almost pure thrusting and the two possible slip-vector azimuths differ by $< 10^\circ$, so we have averaged them. For the western event in the north (grey arrow), we chose the azimuth consistent with nearby GPS data. For the eastern event in the Dzhungarian Alatau (grey arrow), we chose the right-lateral one, which is consistent with the orientation of the mapped faults.

2.3. Seismicity

Historical records of seismicity from this part of central Asia only cover the past ~ 300 years. Only two strong historical events can reliably be tied to individual faults (Figure 1b). The 1889 Chilik (russ. Шелек) earthquake with a magnitude of M_w 8.0–8.3 produced ~ 175 km of surface ruptures in the mountains south of the Ili Basin (Abdrakhmatov et al., 2016). In 1911, the M_w 7.8–7.9 Chon-Kemin earthquake (also referred to as the Kebin earthquake) resulted in almost 200 km of surface ruptures between Almaty and Lake Issyk Kul (Arrowsmith et al., 2017; Bogdanovich et al., 1914). Other significant earthquakes with magnitudes of $M > 7$ such as the 1887 Verny earthquake (Tatevossian, 2007) or the 1978 Dzhalanash-Tyup event (Krüger et al., 2015) did not produce known surface ruptures.

Instrumental seismicity in the Tien Shan is highest along the contact between the Pamir and the Tien Shan in the SW and along its southern margin bordering the Tarim Basin. Relatively few earthquakes with well-constrained depths, mechanism, and locations are available to allow further insights into the regional tectonics in our study area (Maggi et al., 2000; Figure 3). Sloan et al. (2011) determined depths and focal mechanism from teleseismic body wave form inversion of earthquakes with magnitude $> M_w 5$. Craig et al. (2012) used array-waveform modeling to determine the depths of three earthquakes ($M_{4.7}$ – $M_{5.3}$) near Kapchagay. Alinaghi and Krüger (2014) used seismic array analysis for the redetermination of depths of earthquakes in parts of the Tien-Shan, and we used body wave modeling to estimate source parameters of additional post-2011 events, using the MT5 inversion modeling procedure described by Sloan et al. (2011). Details on the parameters of these earthquakes can be found in Figures S1 and S2 and Table S1 in the supporting information. These data reveal a clear pattern of earthquake depth distribution. On the south side of the Tien Shan, at the Tarim margin, thrust earthquakes go down to about 35 km and even deeper within the Tarim Basin itself (Ainscoe et al., 2017). On the north side, within the Kazakh platform, earthquakes occur at depths of 24–28 km around Kapchagay and up to 40-km depth further north in the Kazakh platform. Within the Tien Shan range itself,

all significant earthquakes appear to be no deeper than about 20 km. This indicates a thicker seismogenic layer on the margins (in shields or cratonic material) where the strong foreland supports the high mountain topography with a smaller seismogenic thickness: a pattern seen elsewhere in Asia and the Alpine-Himalayan Belt (e.g., Deichmann & Baer, 1990; Jackson et al., 2008; Kastrup et al., 2004; Sloan et al., 2011).

Instrumental earthquakes in the Ili Basin are sparse and do not conspicuously align along structures and therefore, do not allow evaluating the activity of single faults. Events $> m_b 4.5$ concentrate on the margins of the basin. The few reliable moment tensor solutions available (Figure 3) indicate thrust faulting with earthquake slip vectors directed N to NW. We discuss the relationship between earthquake slip vectors, GPS velocities, and their relationship to our field observations of active faulting in section 4.

3. Active Faulting in the Ili Basin

In the following, we present new data on the active faults within and around the Ili Basin. We first present evidence for recent reverse faulting on the northern margins of the basin. Then we describe the Late Quaternary (re)activation of the large inherited NE-SW trending strike-slip faults, and we finally discuss the role of the NW-SE striking faults in the western part of the basin in more detail.

3.1. E-W Thrust Faults

We investigated the western continuation of the Usek (russ. Усек) thrust, which was studied by Cording et al. (2014). Near the village of Konyrolen (russ. Коньролен) we encountered offset alluvial fans that exhibit a south facing scarp system (site Ko in Figure 1b). The E-W trending scarps are visible in satellite-derived DEMs (SRTM and HMA) and can be traced for more than 30 km (Figure 4a) showing a fairly simple geometry without overlaps. From their intersections with the alluvial fans it is clear that they formed by thrust motion on a north dipping fault system. The scarp is cumulative for most of its length, judging from sites where we found multiple generations of discrete offsets. We produced a high-resolution DEM from overlapping helikite aerial photos to map the scarps in detail and to measure their heights (Figure 4b). We measured maximum vertical offsets of up to 8 m in the center of the rupture (Figures 4c and 4d). Only a few alluvial fans have overprinted the scarps, which points to the offset being a relatively young geomorphological feature. The steepness of several sections of the scarp also indicates that they are likely to be young (Figure 4c). Comparison with known Holocene fault ruptures from nearby sites suggests that the surface offset may be Holocene in age (Campbell, 2015; Grützner, Carson, et al., 2017).

North of the Konyrolen site we investigated the southern Dzhungarian Range Front (russ. Джунгария; Dz in Figure 1b). Here we identified two subparallel, south facing scarps separated by ~1.5 km on satellite imagery and DEMs (Figure 4e). The scarps trend E-W and are >10 and >6 km in length, respectively. In the field we measured a vertical offset of about 15 m across each, which is consistent with measurements made using the HMA DEM (Figures 4e and 4f). The scarps are steep and not heavily eroded or incised, and in places they offset the youngest generations of alluvial fans, but not the present-day river beds (Figure 4g). Based on the amount of vertical offset we speculate that these structures formed in several past reverse-faulting earthquakes within the Late Quaternary, possibly in the Holocene.

Mackenzie (2016) mapped an E-W striking thrust fault east of Shonzhzy, paralleling the Ili River (Figure 1b). This thrust fault has a morphological expression in SRTM1 data. It runs ~30 km north of the Ketmen Range and has a vertical offset of ~25 m in Late Quaternary alluvial fans. This fault is probably a splay fault from the main range-front at the southern margin.

In summary, the large thrust faults bounding the Ili Basin to the north and to the south show evidence of surface rupturing in the late Pleistocene or Holocene. These structures are clearly active, showing that a portion of the overall N-S shortening is accommodated at the margins of the basin.

3.2. NE-SW Strike-Slip Faults

Large NE-SW striking strike-slip faults can be observed in the interior of the mountain ranges surrounding the Ili Basin. The strike-slip faults form a shear zone several hundreds of kilometers in length, but the faults are not continuous across the Ili Basin (Figure 5a). GPS velocities have a small east component in the south of the Ili Basin and a small west component in the north, also indicating left-lateral shear (Figure 2).

At the Altyn Emel (russ. АЛТЫН-ЭМЕЛЬ) mountains, the active Konyrolen thrust fault runs along the southern edge of the E-W mountain front, but the range interior is dominated by a ~120-km-long, NE-SW strike-slip structure cutting the bedrock massif obliquely (Al in Figures 1b and 5b). Horizontal slickensides in bedrock at the SW tip of the fault confirm the left-lateral sense of motion (e.g., 78.598002°E, 44.207950°N). This fault clearly dominates the regional morphology and forms a sharp linear feature across which left-lateral offsets of ~500 m are the most prominent. We used satellite-derived DEMs and field mapping to characterize the geometry and sense of motion of the fault (Figure 5b). At the northeastern tip of the fault zone, the drainage pattern is controlled by the fault. Here uplifted and dissected alluvial fans are present SE of the Altyn Emel Fault, while to its NW the topography is low-lying and flat (Figure 5b). Ridges and elongated compressional structures mark the trace of the fault. In its central part, the fault trace is expressed as a remarkably sharp lineament in the Paleozoic bedrock with the ridge crest of the mountain range being left-laterally offset (Figure 5b). Near the SW end of the fault, the fault trace can be identified from a series of left-laterally displaced channels and springs that emerge from the fault (Figures 5c and 5d). Left-laterally displaced, steep channels show ~2-m horizontal displacements (Figure 5e). A vertical fault scarp of 0.5–1-m height in alluvial material testifies to Late Quaternary, probably Holocene, motion (Figures 5c and 5e).

The left-lateral Chilik-Chon-Kemin Fault system offsets bedrock-incised channels by several hundreds of meters (Figures 6a and 6b) to the southwest of the Bartogai reservoir. Here SE-side-up vertical motion can

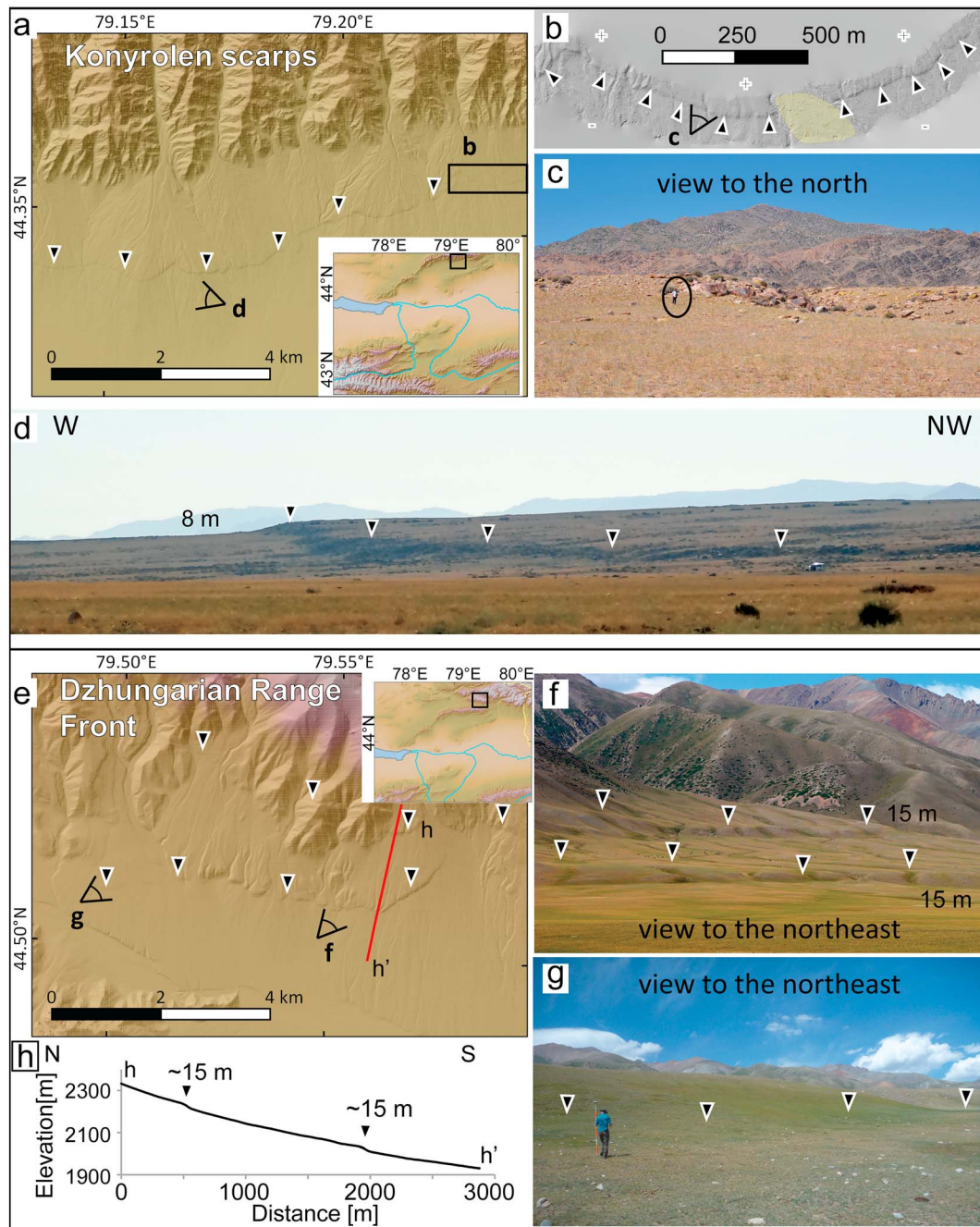


Figure 4. Active thrust faults at the northern edge of the Ili Basin. (a) DEM of a section of the Konyrolen scarps (Ko in Figure 1b; see inset for location). Topography is from the High Mountain Asia 8-meter DEM (HMA; Shean, 2017); holes were filled with SRTM1 data. The rectangle indicates the area covered in Figure 4b. Triangles here and in the following figures mark the fault trace. (b) High-resolution hillshade of a DEM from helikite imagery. An alluvial fan postdating (=covering) the scarp is highlighted in yellow. (c) Field photograph of a 5-m-high section of the scarp (person encircled for scale). Note the size of the boulders in the alluvial fan material. (d) Field photograph of the highest part of the scarp. (e) DEM of a section of the Dzhungarian Range Front scarps (Dz in Figure 1b; see inset for location). Topography is from HMA; holes were filled with SRTM1 data. Red line marks the profile shown in Figure 4h. (f) Panoramic view of the double scarps delineated in Figure 4e. (g) Detail of the southern scarp, person for scale. (h) The two scarps show up in the HMA elevation profile, location in Figure 4e.

also be observed. Around the Bartogai reservoir, displaced channels and deformed gravels in a Late Quaternary alluvial fan prove recent fault activity (Grützner, Carson, et al., 2017). We also observe displaced channels and ridges (Figures 6c and 6d) in high relief SW of the Bartogai reservoir. Here the fault can be traced as a sharp break in slope for several kilometers, and lateral offsets of several tens of meters are preserved in the landscape. The smallest offsets amount to less than 5 m only.

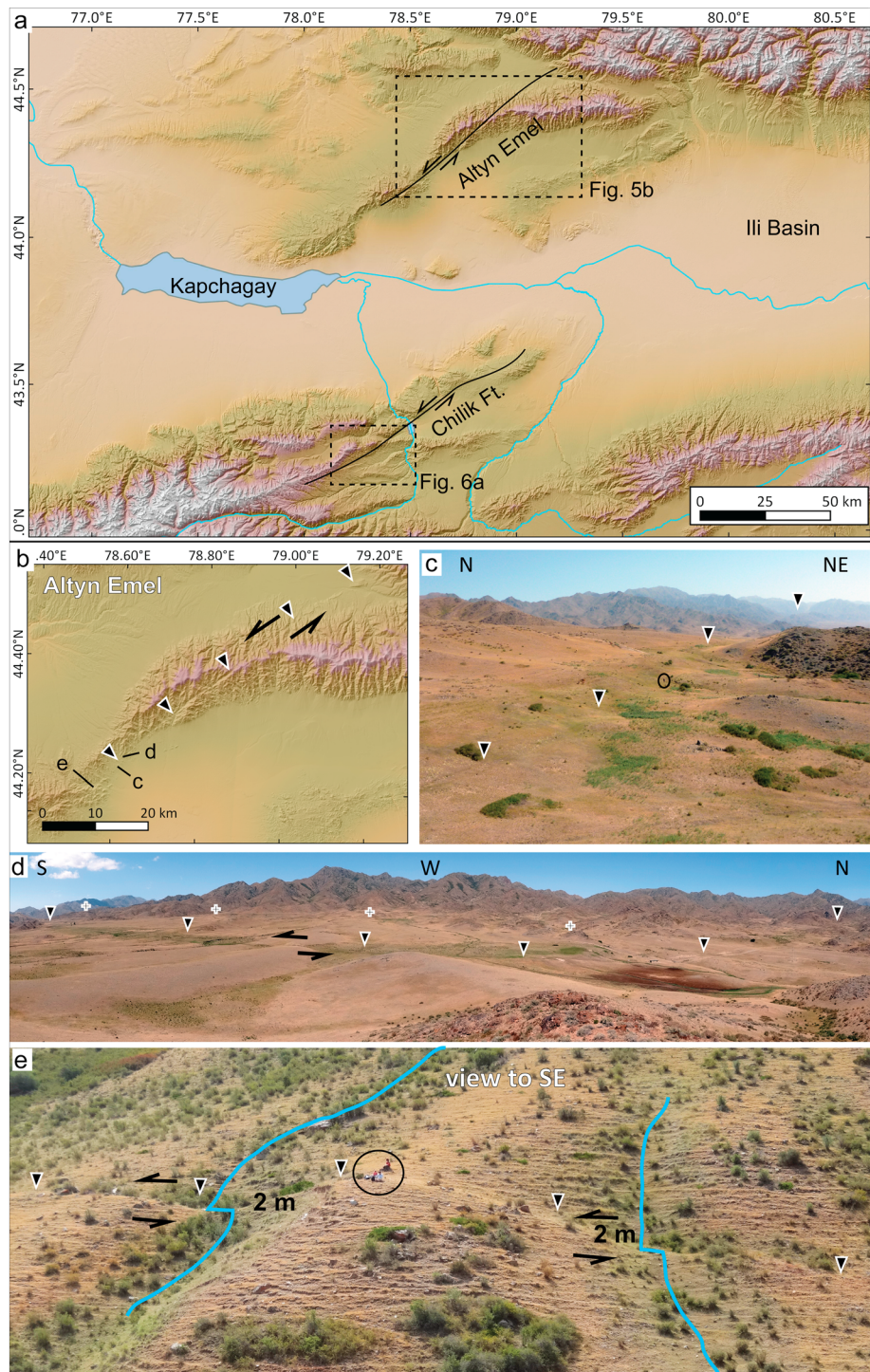


Figure 5. Left-lateral strike slip faults in the study area. (a) Overview of the Altyn Emel and Chilik Fault systems. (b) Trace of the left-lateral Altyn Emel Fault (Al in Figure 1b). Topography is from HMA; holes were filled with SRTM1 data. (c) The fault trace is visible in the youngest alluvium as a line of springs and in the morphology; note the vertical component of motion. Photo location: 78.596921°E, 44.211966°N. Person encircled for scale. (d) Alluvial fans and thalwegs are left-laterally offset by the Altyn Emel Fault. Photo location: 78.606831°E, 44.223262°N. (e) Left-lateral offsets of 2 m observed in channels (blue lines). Two scientists encircled for scale. Photo location: 78.545146°E, 44.189363°N.

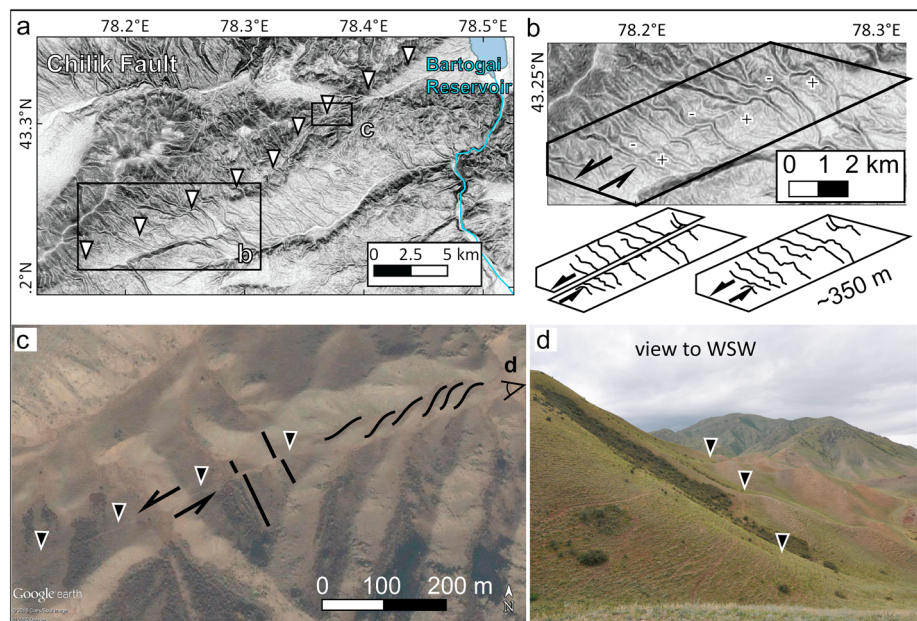


Figure 6. (a) Trace of the Chilik Fault Zone in the SRTM1 slope map. (Ch in Figure 1b). (b) Large-scale horizontal displacement of bedrock incised channels at the Chilik Fault Zone. Although the higher topography is on the NW side of the fault, the SE side is uplifted in the short term. About 350 m of left-lateral displacement can be reconstructed from the channel thalwegs. (c) Left-lateral offsets in ridges and sigmoidal landscape features along the trace of the Chilik Zone. We also note a vertical component of motion (SE side up) in the field. GoogleEarth CNES/SPOT imagery. (d) Field photo of the Chilik Fault trace. Photo location: 78.400623°E, 43.313203°N.

The Altyn Emel Fault and the Chilik-Chon-Kemin Fault system are not aligned, but overlap with an ~60-km left step across the Ili Basin. Remote sensing and field mapping indicate no morphological evidence for NE-SW striking faults in between these two major NE-SW striking structures, and neither instrumental nor historical seismicity indicate left-lateral faulting between them. GPS data, however, indicate left-lateral shear at the western basin margin (Figure 2).

In summary, NE-SW trending left-lateral faults can be traced for hundreds of kilometers in the western Ili Basin. Left-lateral offsets of all scales are preserved in the landscape, ranging from few meters of offset probably related to Holocene single events up to several hundreds of meters of offset seen in deflected channels. Furthermore, the 1889 Chilik earthquake testifies to the activity of this system, although it did not rupture the fault trace with the obvious left-lateral steps in the geomorphology, but a section near Saty (Figure 1b; Abdrakhmatov et al., 2016). Remarkably, this large shear zone is not continuous across the Ili Basin, but seems to be confined to the basement-cored uplifted mountain ranges. We will further elaborate on this important observation in section 4.

3.3. NW-SE Faulting at the Western Basin Margin

A set of subparallel NW-SE striking faults can be observed at the western margin of the Ili Basin (Figure 1b). These faults are shorter in length and much more numerous than the other fault types. In order to establish their morphology and activity, we discuss the three examples of Kalinino (russ. Калинино; Ka in Figure 1b), Kapchagay (russ. Капшарай; Kc in Figure 1b), and Shonzhy (russ. Чунджа; Sh in Figure 1b) in detail.

We mapped numerous NW-SE striking faults of 5–20-km lengths south of the Altyn Emel range (Figure 1b). The faults are subparallel with a spacing of 3–15 km. In the area of Kalinino (Figure 7a), faults offset outcrops of bedrock right-laterally (Kober et al., 2013; Figure 7b), but the age of these offsets is poorly constrained. Where these faults continue into alluvial fans, alluvial fans have been uplifted and vertically offset. Other faults vertically offset alluvial and fluvial surfaces. Those can be recognized in the DEMs and in field photographs (Figure 7). Near Kalinino, we document a fault scarp more than 5 km long and up to 12 m high in the loess-covered basin (Figure 7c). A topographic profile from SRTM data reveals

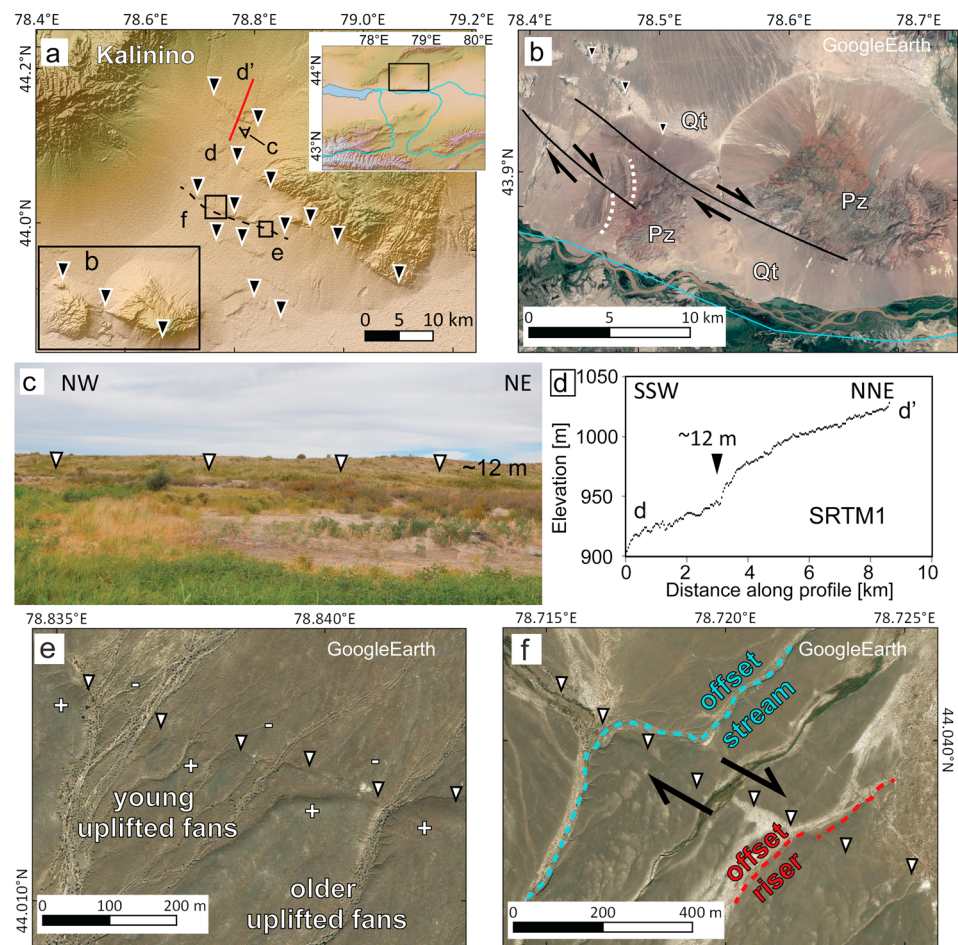


Figure 7. Active deformation at NW-SE striking, right-lateral strike slip faults at the western basin margin, Kalinino site. (a) Surface expression of active faulting near Kalinino, hillshade, and DEM based on HMA and SRTM1 data. Red line marks the SRTM1 elevation profile shown in Figure 7d; triangles mark scarps in the basin fill. Black dashed line is the fault shown in Figures 7e and 7f. (b) Satellite image of offset Paleozoic bedrock ridges near Kalinino. The faults offsetting the bedrock also affect the Quaternary alluvial fans and the drainage. GoogleEarth DigitalGlobe/CNES. (c) Field photo of the ~12-m-high fault scarp near Kalinino. View is from the south to the scarp crossed by the red line in Figure 7a. The footwall and the hanging wall are covered in loess of unknown thickness. Photo location: 78.766408°E, 44.157308°N. (d) SRTM1 elevation profile, location marked by the red line in Figure 7a. The DEM reveals up to 12 m of vertical offset in the youngest sediments. (e) At least two generations of alluvial fans are cut by the fault marked with a dashed line in Figure 7a, which exhibits a vertical component here (south up). GoogleEarth DigitalGlobe/CNES. (f) Fault section with mainly horizontal offsets. Both the recent streams and an older riser show right-lateral displacement. GoogleEarth DigitalGlobe/CNES.

that the vertical offset is not due to local (anthropogenic) modification, but represents a systematic displacement of the basin surface (Figure 7d). Uplifted loess units can be found in the hanging walls of most of those basin faults.

These NW-SE faults affect Late Quaternary abandoned alluvial fan surfaces and control the drainage pattern. For example, an 18-km-long fault trending N110E shows a long-term uplift of loess units north of the fault and springs emerge from the fault scarp. In the center of the fault, right-lateral offsets of several tens of meters can be identified in stream channels and risers of abandoned Quaternary terraces (Figures 7e and 7f). The south-eastern section of the fault affects different generations of alluvial fans (Figure 7e). At some locations we identify south-up vertical displacements against the overall drainage direction (Figure 7e), while neighboring fans show uplift north of the fault. These variations in uplift direction over short distances and the right-lateral displacements indicate that this fault accommodates not only vertical motion but also a significant portion of right-lateral shear.

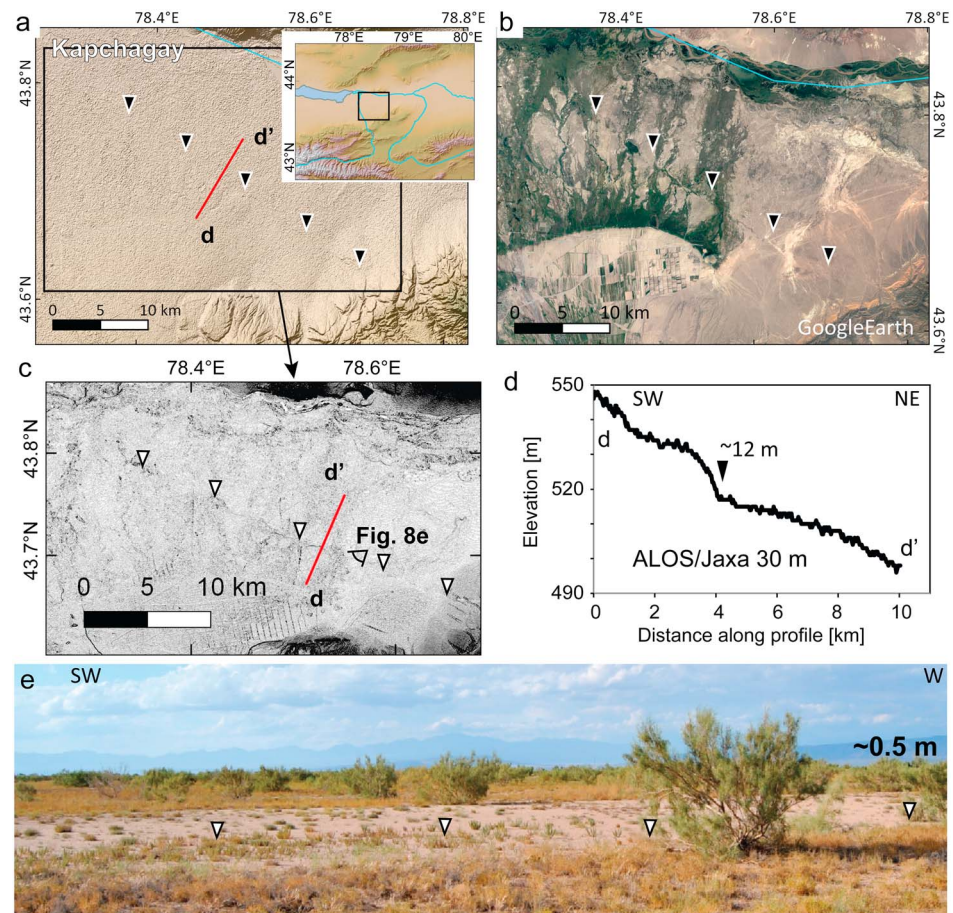


Figure 8. Active deformation at a NW-SE striking fault at the western basin margin, Kapchagay site. (a) A faint, NW-SE trending lineament is just visible in SRTM1 elevation and hillshade data (triangles). Rectangle marks the extent of Figure 8c, red line marks the profile line in Figure 8d, and inset shows the location within the Ili Basin. (b) Satellite image of the same area as in Figure 8a. Note the change in vegetation along the fault in the basin. GoogleEarth DigitalGlobe/CNES imagery. (c) ALOS/Jaxa (30-m resolution) hillshade map of the area marked in Figure 8a. Note that despite the higher noise level compared to SRTM1, the lineament is clearly discernible. (d) ALOS/Jaxa elevation profile, location marked by the red line in Figure 8a. The DEM reveals up to 12 m of vertical offset. (e) Field photograph of the scarp, vertical offset is ~0.5 m. View is to the SW, location marked in Figure 8c; 43.673321°N, 78.611516°E.

Several arguments suggest that most of the NW-SE faults in the Ili Basin are at least partly right-lateral: (i) the orientation of these NW-SE trending faults with respect to the overall N-S shortening implies that they accommodate a component of right-lateral deformation, although some of these faults are running perpendicular to the horizontal shortening direction derived from GPS; (ii) there is vertical offset in the Paleozoic bedrock (Kober et al., 2013), but also significant right-lateral displacement; (iii) we see right-lateral offsets in Quaternary landforms such as terrace risers and streams; and (iv) we observe clear right-lateral offsets in similarly oriented faults in neighboring basins that are under the same present-day stress regime (see Campbell et al. (2013) for the Dzhungarian Fault and Burtman et al. (1996) and Rust et al. (2018) for the Talas-Fergana Fault).

Another NW-SE striking fault with vertical offset was found SE of the Kapchagay reservoir (Kc in Figure 1b). The fault runs NW-SE and can be traced for around 40 km in the DEM (Figure 8a) and in optical satellite imagery (Figure 8b). In this case, the slope map derived from 30-m JAXA elevation data (Figure 8c) reveals the surface expression of active faulting much clearer than the SRTM1 data set, despite the higher noise level. The basin floor is vertically offset by up to 20 m in the center of the fault, exhibiting a wide deformation zone, which may be a result of modification by high sediment flux (Figure 8d). We observe a relatively sharp offset where the scarp is visible in the optical imagery.

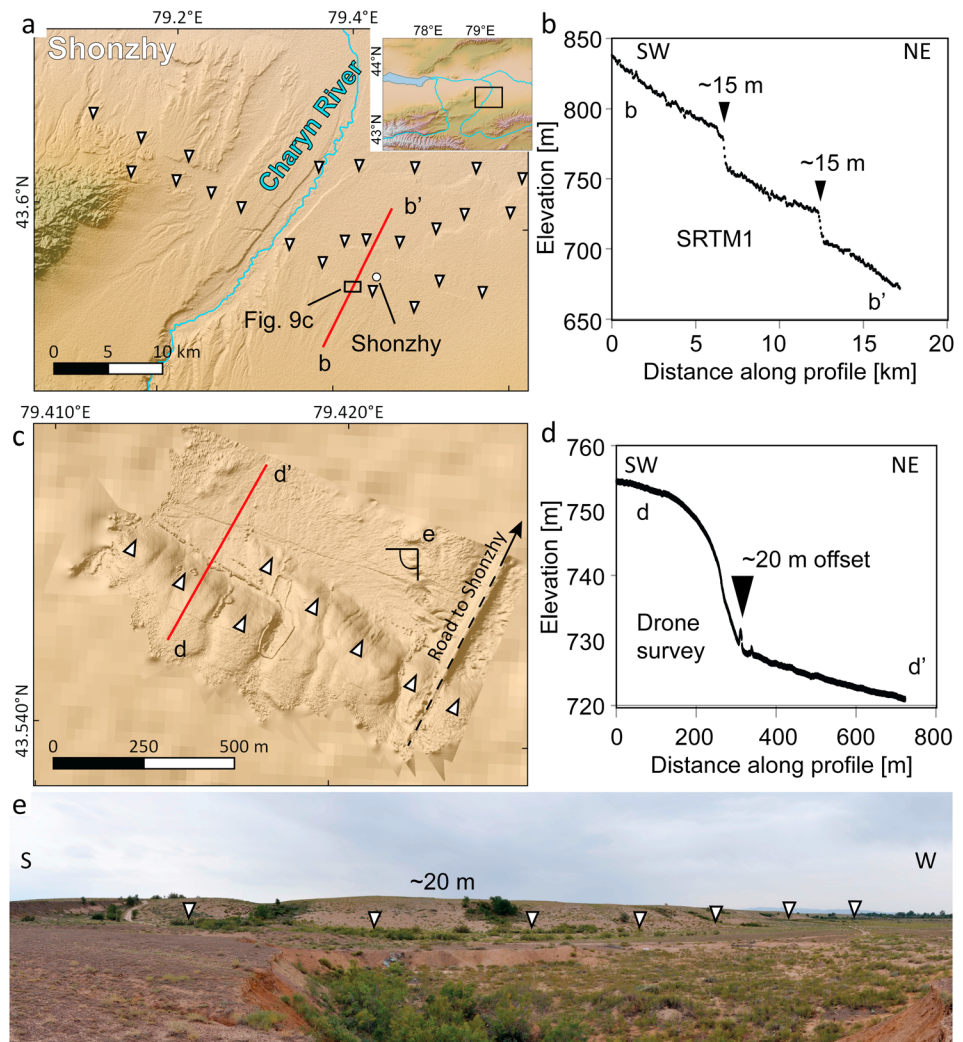


Figure 9. Active deformation at a NW-SE striking fault in the basin interior, Shonzhy site. (a) Surface expression of active faulting near the city of Shonzhy, hillshade, and DEM based on HMA and SRTM1 data. Red line marks the SRTM1 elevation profile shown in Figure 9b; triangles mark scarps in the basin fill. The faults affect Quaternary alluvial fans. (b) SRTM1 elevation profile, location marked by the red line in Figure 9a. The DEM reveals up to ~30 m of cumulative vertical offset across two main scarps, probably in the Late Quaternary. (c) Drone DEM of the Shonzhy scarp, see location in Figure 9a. (d) The elevation profile from SfM drone data across the scarp near Shonzhy reveals ~20 m of vertical offset. (e) Panoramic field photograph of the Shonzhy scarp where it is the highest (~20-m vertical offset). View is to the SW, same site as the drone DEM in Figure 9c.

We inspected the site with the sharp offset in the field and encountered a small fault scarp of ~0.5-m height only. The scarp offsets young alluvial material and loess in the otherwise low-relief basin interior. This offset must be recent and is interpreted as the surface expression of a single large earthquake that most likely occurred in the Holocene (Figure 8e). It is intriguing that the observed single-event offset is only 0.5 m in the field, while much larger displacements can be identified across this same structure in remote sensing data. This observation stresses the importance of combining different approaches when mapping active faults.

In the southern part of the Ili Basin, NW-SE striking faults are present around the town of Shonzhy (Figure 9a). The entire set of faults has a length of ~40 km and is bordered in the east by a long E-W reverse fault that parallels the Ili River. In the northwest, the longest of those faults bounds bedrock against basin sediments. We also observe faults that offset Paleozoic bedrock units by several hundreds of meters, but we exclude these from our mapping because we cannot narrow down the age of their most recent activity. SRTM1 elevation data along a profile near the city of Shonzhy reveal two main fault scarps with vertical

offsets of several tens of meters (Figure 9b). The most prominent NE facing scarp was encountered west of Shonzhy (Sh in Figures 1b and 9c). We measured a vertical displacement of more than 15 m with DGPS, which was confirmed by a drone survey and SRTM1 data (Figure 9d). A thick loess cover in the SW of the scarp is probably of Holocene age (Figure 9e). The scarp can be traced for several kilometers and has only a few minor left steps (Figure 9c). At most places along strike we found a loess cover on both sides of the fault. Fine to medium gravels are present on the footwall surface where the offset is largest, which may indicate that fluvial activity has contributed to the overall scarp height. Springs are visible all along fault strike. We cannot identify horizontal motions along the faults here, but the vertical motion is evident in the drainage pattern as streams are often deflected by, or terminate at, the faults all around Shonzhy. For the same reasons as discussed in the case of Kalinino, we speculate that at least some right-lateral shear is taken up by the faults near Shonzhy site.

In summary, NW-SE trending faults with lengths of 5–40 km are present in the interior of the Ili Basin. They offset Late Quaternary and even Holocene strata, and they control the most recent drainage. We infer that these structures accommodate vertical, but also right-lateral motion for several reasons: (i) they right-laterally offset Paleozoic bedrock; (ii) their orientation with respect to the present-day stress field indicates right-lateral slip; and (iii) from morphological arguments including displaced and offset alluvial fans, terrace risers, and stream channels. These basin-interior faults close the gap between the large NE-SW trending, left-lateral shear zones north and south of the Ili Basin; that is, they accommodate the remaining deformation between the two major NE-SW strike-slip systems of Altyn Emel and Chilik. In the following we will especially stress this last observation and discuss their role in the overall N-S contractional setting.

4. Discussion

4.1. Field Observations

Our field studies lead to two main observations. First, the active deformation in our study area in the northern Tien Shan is not limited to E-W striking thrust faults perpendicular to the shortening direction. We find an additional large-scale zigzag pattern with large NE-SW left-lateral strike-slip faults in the Paleozoic mountain ranges, and a right-lateral component of motion on numerous NW-SE trending oblique thrust faults mainly in the basin interior. All of these faults have a vertical component of motion and show Late Quaternary/Holocene offsets. Second, we observe that shortening across the Ili Basin is not limited to the basin-bounding ranges, but is also accommodated on the NW margin of the basin by faulting (and folding; see Kober et al., 2013). This is in agreement with the decline of N-S GPS velocities toward the north (Zubovich et al., 2010; Figure 2). E-W GPS velocities change from 1 mm/year eastward to 1 mm/year westward (Zubovich et al., 2010), which is also in agreement with the trend of the large NE-SW strike-slip fault system (Figure 2) that constitutes a major, but rather slowly deforming shear zone.

4.2. Insights From GPS and Earthquakes

At the longitude of our study area the GPS velocities in the Ili Basin are east of north, but in the Dzhungarian Alatau they are west of north. The slip vectors of earthquakes in the south of the basin are west of north, and so are the ones to the north in the Dzhungarian Alatau (Figure 3). The right-lateral nodal plane of the well-constrained fault plane solution near Tekeli (M_w 5.4 in 1993, 15-km depth; from Sloan et al., 2011; black moment-tensor solution west of the Dzhungarian Alatau in Figure 3) can be interpreted as slip on a right-lateral, NW-SE striking fault. In this case the earthquake slip vector parallels the GPS velocity. This overall setting requires left-lateral NE-SW faulting on the NW margin of the Ili Basin. The earthquake slip vectors are, therefore, consistent with the GPS (though different from the GPS velocity vectors themselves, which are relative to stable Eurasia) and the interpretation of our field observations.

We constructed a velocity triangle to summarize these observations (Figure 10a): the Tarim block moves north relative to Eurasia at about 20 mm/year at the longitude of the Ili Basin, based on GPS data. GPS velocities and earthquake slip vectors show that the south side of the Dzhungarian Alatau moves in direction 345 relative to Eurasia. The Ili Basin is moving in direction 165 relative to Tarim (or Tarim at 345 relative to Ili), based on slip vectors of thrusts along the Tarim margin. The earthquake slip vector south of the Ketmen Range at 17-km depth (Figure 3) is representative of others along the Tarim margin further south. These two directions are therefore approximately parallel. This indicates that the minimum movement between the

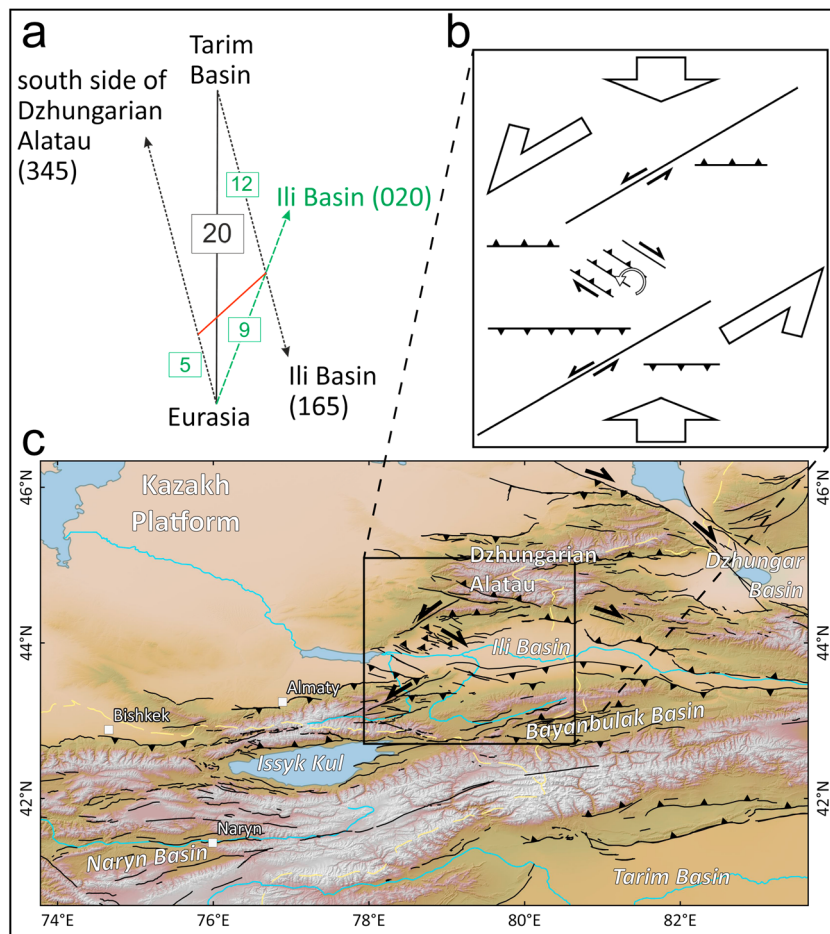


Figure 10. (a) The velocity triangle summarizes the relative motions of the Tarim Basin, the Ili Basin, and the Dzhungarian Alatau with respect to stable Eurasia. Velocities in mm/year (in rectangles) and directions (in brackets) are from GPS data (Zubovich et al., 2010) and earthquake slip vectors discussed in this paper. (b) Cartoon summarizing our findings and illustrating the proposed model of deformation. E-W thrust faults bound the ranges. Large NE-SW strike-slip faults in the range interiors are left-lateral, and smaller conjugate NW-SE faults mainly in the basin have a right-lateral oblique sense of motion. The right-lateral faulting occurs within a gap in the left-lateral faults, and we infer that they accommodate the left-lateral shear by counterclockwise vertical-axis rotation. (c) The Ili Basin and its unique deformation style in the regional framework.

Dzhungarian range and the Ili Basin is in azimuth 075 at a rate of about 5 mm/year. For the direction NE ($A_z = 045$) this motion is around 6 mm/year. This also means that the north side of the Ili Basin is moving in direction 020 relative to Asia (green line in Figure 10a). The expected convergence rate between the Ili Basin and Eurasia is about 9 mm/year, and between Ili and Tarim about 12 mm/year. If the motions between Ili and the Dzhungarian Alatau were accommodated on a NE trending left-lateral fault (red line), the Dzhungarian Alatau would be moving about 5 mm/year toward Eurasia. Although a literal interpretation of this simplified model requires rigid blocks moving along single faults, which is clearly not the case in our study area, it is sufficient to illustrate the overall tectonic picture and the motions are in accordance with the field observations.

4.3. The Role of the Oblique Right-Lateral, NW-SE Faults

A possible role of the oblique right-lateral faults is to consume N-S shortening not only by their vertical motion but also by rotations about vertical axes in the region between the offset in the left-lateral strike-slip faults. The Ili basin is sited in a left-stepping gap between the large NE-SW striking left-lateral faults. Within the basin we found sets of smaller NW-SE faults that abut, but do not truncate, the main left-lateral faults; most of them have recently been active. These faults were found to bridge the gap in the NE-SW trend that

exists at the Ili Basin. A counterclockwise rotation of these oblique right-lateral faults about vertical axes would not only transfer the left-lateral deformation across the Ili Basin but also allow for the accommodation of regional N-S shortening, as well as accommodating localized NE-SW extension within the step-over between the two main left-lateral fault segments. Additional shortening is taken up by internal deformation of the area in between these faults, that is, by folding as observed in the Ili Basin (Kober et al., 2013), and by the vertical component of motion that is evident from our data. Such kinematics would require little overall E-W divergence, which fits the GPS observations (Figures 2 and 3). It also explains the role of the large NE-SW structures that act as a major shear zone. This indicates that no rotation occurs on the NE-SW striking faults, which is supported by the high relief of the areas that exhibit left-lateral faulting like the Altyn Emel range and the Chili-Chon-Kemin Fault zone.

We therefore favor a model with rotation of faults on the NW margin of the western Ili Basin to explain the ongoing deformation in our study area (Figures 10b and 10c). Here strike-slip faults contribute to the overall shortening in a rather simple configuration, and they take up the NE-SW shear.

Vertical axis rotations of strike-slip faults in contractional and transpressional settings have been observed in other parts of the Alpine-Himalayan Belt, for example, in Iran. Freund (1970) described the rotation of conjugate strike-slip faults as a result of compression in southeastern Iran. Several geodetic, geomorphological, and seismological studies show the importance of vertical axis rotations to accommodate shear and compression (e.g., Jackson & McKenzie, 1984; Walker & Jackson, 2004; Walpersdorf et al., 2014). Mattei et al. (2012) used paleomagnetic data to measure block rotations associated with active faults in central Iran; Hollingsworth et al. (2006) describe a set of counterclockwise rotating blocks in the Kopeh Dagh Mountains. This style of deformation seems to be common in regimes of transpression. Although it is widely reported that large-scale block rotations have played an important role in the formation of the Tien Shan as a whole (e.g., Avouac et al., 1993; Thomas et al., 1993; van der Voo et al., 2006), only few studies discussed the role of active fault rotations about a vertical axis in the accommodation of the overall shortening (for the Dzhungarian Fault: Campbell et al., 2013). Our study is the first to look at the role of rotating strike-slip faults in an actively deforming basin with a variety of different methods. We emphasize the need to integrate observations from seismology, geodesy, geology, and geomorphology to constrain the regional tectonic picture. Each method has its own uncertainties, but together they combine to draw a coherent and consistent picture.

4.4. Implications for the Regional Tectonics

The almost aseismic behavior of the Ili Basin and the fact that its wide, flat area is surrounded by mountain ranges that have experienced significant uplift, supports the assumption that its lithosphere is different, or has different rheological properties, from that in the high ranges of the Tien Shan. The Tarim Basin behaves as a largely aseismic block that mainly deforms at its margins (e.g., Thompson Jobe et al., 2017) and only partly in its interior (Mazar Tagh Fault System; Pan et al., 2010). This is in stark contrast to the surrounding mountain ranges and indicates strong Tarim lithosphere (e.g., Neil & Houseman, 1997). The same holds true for the Dzhungar Basin that bounds the Borohoro Shan to the northeast (Allen et al., 1991; Allen & Vincent, 1997). Lake Issyk Kul also shows relatively weak seismicity compared with the surrounding ranges. The bathymetry and the topography along its edges further indicate a fundamental difference in the crustal material, although recent seismic surveys have shown that the lake floor is deforming (Buslov et al., 2003; de Batist et al., 2002; Gebhardt et al., 2017). Issyk Kul may be the relict of a stronger block trapped between weaker units (e.g., Buslov et al., 2003) that have recently entered a stage where it is easier to deform the interior rather than further uplift the surrounding mountains which reach over 5,000 m above sea level. We speculate that the Ili Basin may have reached a similar stage. The basement geology of the Ili Basin includes fragments of microcontinents and amalgamated island arcs, with an Early Proterozoic basement (Allen et al., 1993; Charvet et al., 2011; Gao et al., 2009; Heubeck, 2001; Şengör et al., 1993; Windley et al., 2007; Zhang et al., 1984) that is likely relatively strong. The oblique right-lateral faults on the NW margin of the Ili Basin interior show the onset of deformation within the basin interior.

The primary cause of the zigzag pattern that we observe might be found in the reactivation of inherited, probably Permian, tectonic structures (Allen et al., 1995; Jolivet et al., 2010; Selander et al., 2012). In the case of the large NE-SW striking strike-slip faults such as the Chilik-Chon-Kemin Fault and the Altyn Emel this also explains the morphology and offsets in the Paleozoic bedrock. Whether or not the basin-interior oblique

right-lateral faulting also follows preexisting structures is less clear. Kober et al. (2013) show that at least some of these faults are reactivated, older structural features. However, most of the observed right-lateral offsets seen today could have also been accumulated during the Cenozoic.

Interestingly, the 1889 Chilik earthquake surface ruptures illustrated that a zigzag pattern of strike-slip and reverse faulting can be generated at large scale when preexisting faults are reactivated in a single great earthquake (Abdrakhmatov et al., 2016), so perhaps it is no coincidence that we observe a zigzag pattern in the longer-term topography and structure. The Ili Basin is a special case: it is a rigid continental sliver like the Tarim and the Dzhungar Basin, but its unique position in between the high neighboring ranges and its complex deformation history during the different phases of mountain building have weakened the crust and probably reactivated inherited structures. Therefore, its present-day deformation style is very different from that of the Tarim and the Dzhungar Basins, and it may illustrate how even strong microcontinents ultimately get crushed in the Alpine-Himalayan collision zone.

5. Conclusions

Careful fault mapping from remote-sensing data and DEMs derived from satellite and aerial imagery, field surveys, and DGPS allowed us to reveal the pattern of active deformation in the Ili Basin area of the northern Tien Shan. Our observations and interpretations are supported by GPS and earthquake data. The combination of these different methods allows drawing a coherent picture of the active deformation. We found that inherited NE-SW striking left-lateral faults in the Paleozoic ranges accommodate large-scale NE-SW shear, and that NW-SE striking oblique right-lateral faults are active in the western basin margin. Around 6 mm/year of NE-SW left-lateral shear is accommodated across the entire study area; ~3 mm/year are taken up at the NW margin of the Ili Basin. E-W striking thrust faults are mainly present at the boundaries of the basin. Regional N-S shortening is accommodated by dip-slip components on all three fault types, and also by counterclockwise rotation of the oblique right-lateral strike-slip faults about vertical axes away from the direction of main horizontal compression. It is likely that the conjugate strike-slip faults at least partly reactivate inherited tectonic structures. The Ili Basin has started to deform internally, although it is made up of rather strong continental crust. In contrast to other intramontane basins in the Tien Shan such as Naryn or Bayanbulak, strike-slip deformation plays an important role in the Ili Basin.

References

- Abdrakhmatov, K., Walker, R. T., Campbell, G. E., Carr, A. S., Elliott, A., Hillemann, C., et al. (2016). Multi-segment rupture in the July 11th 1889 Chilik earthquake (M_w 8.0–8.3), Kazakh Tien Shan, identified from remote-sensing, field survey, and palaeoseismic trenching. *Journal of Geophysical Research: Solid Earth*, 121, 4615–4640. <https://doi.org/10.1002/2015JB012763>
- Abdrakhmatov, K. Y., Aldazhanov, S. A., Hager, B. H., Hamburger, M. W., Herring, T. A., Kalabaev, K. B., et al. (1996). Relatively recent construction of the Tien Shan inferred from GPS measurements of present-day crustal deformation rates. *Nature*, 384(6608), 450–453. <https://doi.org/10.1038/384450a0>
- Ainscoe, E. A., Elliott, J. R., Copley, A., Craig, T. J., Li, T., Parsons, B. E., & Walker, R. T. (2017). Blind thrusting, surface folding, and the development of geological structure in the M_w 6.3 2015 Pishan (China) earthquake. *Journal of Geophysical Research: Solid Earth*, 122, 9359–9382. <https://doi.org/10.1002/2017JB014268>
- Alinaghi, A., & Krüger, F. (2014). Seismic array analysis and redetermination of depths of earthquakes in Tien-Shan: Implications for strength of the crust and lithosphere. *Geophysical Journal International*, 198, 1111–1129. <https://doi.org/10.1093/gji/ggu141>
- Allen, M. B., Şengör, A. M. C., & Natal'in, B. A. (1995). Junggar, Turfan and Alakol basins as Late Permian to ?Early Triassic extensional structures in a sinistral shear zone in the Altaid orogenic collage, Central Asia. *Journal of the Geological Society*, 152(2), 327–338. <https://doi.org/10.1144/gsjgs.152.2.0327>
- Allen, M. B., & Vincent, S. J. (1997). Fault reactivation in the Junggar region, northwest China: The role of basement structures during Mesozoic-Cenozoic compression. *Journal of the Geological Society*, 154(1), 151–155. <https://doi.org/10.1144/gsjgs.154.1.0151>
- Allen, M. B., Vincent, S. J., & Wheeler, P. J. (1999). Late Cenozoic tectonics of the Kepingtage thrust zone: Interactions of the Tien Shan and Tarim Basin, northwest China. *Tectonics*, 18(4), 639–654. <https://doi.org/10.1029/1999TC900019>
- Allen, M. B., Windley, B. F., Chi, Z., Zhong-Yan, Z., & Guang-Rei, W. (1991). Basin evolution within and adjacent to the Tien Shan Range, NW China. *Journal of the Geological Society*, 148(2), 369–378. <https://doi.org/10.1144/gsjgs.148.2.0369>
- Allen, M. B., Windley, B. F., & Zhang, C. (1993). Palaeozoic collisional tectonics and magmatism of the Chinese Tien Shan, central Asia. *Tectonophysics*, 220(1–4), 89–115. [https://doi.org/10.1016/0040-1951\(93\)90225-9](https://doi.org/10.1016/0040-1951(93)90225-9)
- Arrowsmith, J. R., Crosby, C. J., Korzhenev, A. M., Mamurov, E., Povolotskaya, I., Guralnik, B., & Landgraf, A. (2017). Surface rupture of the 1911 Kebin (Chon-Kemin) earthquake, northern Tien Shan, Kyrgyzstan. *Geological Society, London, Special Publications*, 432(1), 233–253. <https://doi.org/10.1144/SP432.10>
- Avouac, J. P., & Tapponnier, P. (1993). Kinematic model of active deformation in central Asia. *Geophysical Research Letters*, 20(10), 895–898. <https://doi.org/10.1029/93GL00128>
- Avouac, J. P., Tapponnier, P., Bai, M., You, H., & Wang, G. (1993). Active thrusting and folding along the northern Tien Shan and late Cenozoic rotation of the Tarim relative to Dzungaria and Kazakhstan. *Journal of Geophysical Research*, 98(B4), 6755–6804. <https://doi.org/10.1029/92JB01963>

Acknowledgments

This study was made possible by the Earthquakes without Frontiers project (grant code EwF_NE/J02001X/1_1) and the Centre for Observation and Modelling of Earthquakes and Tectonics (COMET). R.T.W. was supported through a University Research Fellowship from the Royal Society of London. Komsat imagery was provided by the European Space Agency through project allocation C1P.6462. The ALOS Global Digital Surface Model (AW3D30) is provided by and is copyright of JAXA. SRTM data are distributed by the Land Processes Distributed Active Archive Center (LP DAAC), located at USGS/EROS, Sioux Falls, SD, <http://lpdaac.usgs.gov>. The High Mountain Asia 8-m DEM is available from the NASA National Snow and Ice Data Center Distributed Active Archive Center (NSIDC DAAC). The drone DEMs will be made available through OpenTopography (www.opentopography.org). This paper is partly based on two PhD theses (Campbell, 2015; Mackenzie, 2016). We thank our field team from Kyrgyzstan and Kazakhstan for their incredible work. Several figures were made with the Generic Mapping Tool software by Wessel and Smith (1998). We thank Marc Jolivet and Stephane Dominguez for their detailed and constructive comments that helped to improve the manuscript.

- Bogdanovich, K. I., Kark, I. M., Korolkov, B. Y., & Mushketov, D. I. (1914). Earthquake in northern district of Tien Shan, 22 December 1910 (4 January 1911). In Russian. Commission of the Geology Committee, St Petersburg, 1914.
- Buckman, S., & Aitchison, J. C. (2004). Tectonic evolution of Palaeozoic terranes in west Junggar, Xinjiang, NW China. *Geological Society, London, Special Publications*, 226(1), 101–129. <https://doi.org/10.1144/GSL.SP.2004.226.01.06>
- Bufe, A., Bekaert, D. P., Hussain, E., Bookhagen, B., Burbank, D. W., Thompson Jobe, J. A., et al. (2017). Temporal changes in rock uplift rates of folds in the foreland of the Tien Shan and the Pamir from geodetic and geologic data. *Geophysical Research Letters*, 44, 10–977. <https://doi.org/10.1002/2017GL073627>
- Bullen, M. E., Burbank, D. W., & Garver, J. I. (2003). Building the northern Tien Shan: Integrated thermal, structural, and topographic constraints. *The Journal of Geology*, 111(2), 149–165. <https://doi.org/10.1086/345840>
- Burbank, D. W., McLean, J. K., Bullen, M., Abdrakhmatov, K. Y., & Miller, M. M. (1999). Partitioning of intermontane basins by thrust-related folding, Tien Shan, Kyrgyzstan. *Basin Research*, 11(1), 75–92. <https://doi.org/10.1046/j.1365-2117.1999.00086.x>
- Burtman, V. S. (2012). Geodynamics of Tibet, Tarim, and the Tien Shan in the late Cenozoic. *Geotectonics*, 46(3), 185–211. <https://doi.org/10.1134/S0016852112030028>
- Burtman, V. S., Skobelev, S. F., & Molnar, P. (1996). Late Cenozoic slip on the Talas-Ferghana fault, the Tien Shan, central Asia. *Geological Society of America Bulletin*, 108(8), 1004–1021. [https://doi.org/10.1130/0016-7606\(1996\)108<1004:LCSOTT>2.3.CO;2](https://doi.org/10.1130/0016-7606(1996)108<1004:LCSOTT>2.3.CO;2)
- Buslov, M. M., Klerkx, J., Abdrakhmatov, K., Delvaux, D., Batalev, V. Y., Kuchai, O. A., et al. (2003). Recent strike-slip deformation of the northern Tien Shan. *Geological Society, London, Special Publications*, 210(1), 53–64. <https://doi.org/10.1144/GSL.SP.2003.210.01.04>
- Campbell, G. E. (2015). Active tectonics of the Tien Shan, central Asia. PhD thesis, Univ. of Cambridge, UK.
- Campbell, G. E., Walker, R. T., Abdrakhmatov, K., Jackson, J., Elliott, J. R., Mackenzie, D., et al. (2015). Great earthquakes in low strain rate continental interiors: An example from SE Kazakhstan. *Journal of Geophysical Research: Solid Earth*, 120, 5507–5534. <https://doi.org/10.1002/2015JB011925>
- Campbell, G. E., Walker, R. T., Abdrakhmatov, K., Schwenninger, J. L., Jackson, J., Elliott, J. R., & Copley, A. (2013). The Dzhungarian fault: Late Quaternary tectonics and slip rate of a major right-lateral strike-slip fault in the northern Tien Shan region. *Journal of Geophysical Research: Solid Earth*, 118, 5681–5698. <https://doi.org/10.1002/jgrb.50367>
- Carroll, A. R., Graham, S. A., Hendrix, M. S., Ying, D., & Zhou, D. (1995). Late Paleozoic tectonic amalgamation of northwestern China: Sedimentary record of the northern Tarim, northwestern Turpan, and southern Junggar basins. *Geological Society of America Bulletin*, 107(5), 571–594. [https://doi.org/10.1130/0016-7606\(1995\)107<0571:LPTAON>2.3.CO;2](https://doi.org/10.1130/0016-7606(1995)107<0571:LPTAON>2.3.CO;2)
- Charreau, J., Saint-Carlier, D., Dominguez, S., Lavé, J., Bland, P. H., Avouac, J. P., et al. (2017). Denudation outpaced by crustal thickening in the eastern Tianshan. *Earth and Planetary Science Letters*, 479, 179–191. <https://doi.org/10.1016/j.epsl.2017.09.025>
- Charvet, J., Shu, L., Laurent-Charvet, S., Wang, B., Faure, M., Cluzel, D., et al. (2011). Palaeozoic tectonic evolution of the Tianshan belt, NW China. *Science China Earth Sciences*, 54(2), 166–184. <https://doi.org/10.1007/s11430-010-4138-1>
- Cording, A., Hetzel, R., Kober, M., & Kley, J. (2014). 10Be exposure dating of river terraces at the southern mountain front of the Dzungarian Alatau (SE Kazakhstan) reveals rate of thrust faulting over the past ~400 ka. *Quaternary Research*, 81(1), 168–178. <https://doi.org/10.1016/j.yqres.2013.10.016>
- Craig, T. J., Copley, A., & Jackson, J. (2012). Thermal and tectonic consequences of India underthrusting Tibet. *Earth and Planetary Science Letters*, 353, 231–239.
- de Batist, M., Imbo, Y., Vermeesch, P., Klerkx, J., Giral, S., Delvaux, D., et al. (2002). Bathymetry and sedimentary environments of Lake Issyk-Kul, Kyrgyz Republic (central Asia): A large, high-altitude, tectonic lake. In *Lake Issyk-Kul: Its Natural Environment*, (pp. 101–123). Dordrecht: Springer. https://doi.org/10.1007/978-94-010-0491-6_9
- Deichmann, N., & Baer, M. (1990). Earthquake focal depths below the Alps and northern Alpine foreland of Switzerland. In *The European Geotraverse: Integrative Studies*, (pp. 277–288). Strasbourg, France: European Science Foundation.
- Dewey, J. F., Shackleton, R. M., Chengfa, C., & Yiyin, S. (1988). The tectonic evolution of the Tibetan Plateau. *Philosophical Transactions of the Royal Society of London. Series A, Mathematical and Physical Sciences*, 327(1594), 379–413. <https://doi.org/10.1098/rsta.1988.0135>
- Engdahl, E., van der Hilst, R., & Buland, R. (1998). Global teleseismic earthquake relocation with improved travel times and procedures for depth determination. *Bulletin of the Seismological Society of America*, 88(3), 722–743.
- Freund, R. (1970). Rotation of strike slip faults in Sistan, southeast Iran. *The Journal of Geology*, 78(2), 188–200. <https://doi.org/10.1086/627500>
- Frisch, K., Voigt, S., Voigt, T., Hellwig, A., Verestek, V., & Weber, Y. (2019). Extreme aridity prior to lake expansion deciphered from facies evolution in the Miocene Ili Basin, south-east Kazakhstan. *Sedimentology*.
- Gao, J., Long, L., Klemd, R., Qian, Q., Liu, D., Xiong, X., et al. (2009). Tectonic evolution of the South Tianshan orogen and adjacent regions, NW China: Geochemical and age constraints of granitoid rocks. *International Journal of Earth Sciences*, 98(6), 1221–1238. <https://doi.org/10.1007/s00531-008-0370-8>
- Gebhardt, A. C., Naudts, L., de Mol, L., Klerkx, J., Abdrakhmatov, K., Sobel, E. R., & de Batist, M. (2017). High-amplitude lake-level changes in tectonically active Lake Issyk-Kul (Kyrgyzstan) revealed by high-resolution seismic reflection data. *Climate of the Past*, 13(1), 73–92. <https://doi.org/10.5194/cp-13-73-2017>
- Goode, J. K., Burbank, D. W., & Bookhagen, B. (2011). Basin width control of faulting in the Naryn Basin, south-central Kyrgyzstan. *Tectonics*, 30, TC6009. <https://doi.org/10.1029/2011TC002910>
- Goryachev, A. V. (1959). *Mesozoic–Cenozoic Structure, History, Tectonic Development, and Seismicity of the Regions of the Lake Issyk-Kul* [In Russian]. Moscow: Academy of Sciences Publishing House.
- Grützner, C., Carson, E., Walker, R. T., Rhodes, E., Mukambayev, A., Moldobaev, A., et al. (2017). Assessing the activity of faults in continental interiors: Palaeoseismic insights from SE Kazakhstan. *Earth and Planetary Science Letters*, 459, 93–104. <https://doi.org/10.1016/j.epsl.2016.11.025>
- Grützner, C., Walker, R. T., Abdrakhmatov, K. E., Mukambayev, A., Elliott, A. J., & Elliott, J. R. (2017). Active tectonics around Almaty and along the Zailiysky Alatau range front. *Tectonics*, 36, 2192–2226. <https://doi.org/10.1002/2017TC004657>
- Han, X. Z., Li, S. X., Zheng, E. J., Li, X. G., Cai, Y. Q., & Chen, Z. L. (2004). Neotectonic activity characteristics of Yiyili Basin and its relation to the formation of sandstone-type uranium deposits. *Xinjiang Geology*, 22(4), 378–381.
- Hellwig, A., Voigt, S., Mulch, A., Frisch, K., Bartenstein, A., Pross, J., et al. (2018). Late Oligocene to early Miocene humidity change recorded in terrestrial sequences in the Ili Basin (south-eastern Kazakhstan, Central Asia). *Sedimentology*, 65(2), 517–539. <https://doi.org/10.1111/sed.12390>
- Hendrix, M. S., Dumitru, T. A., & Graham, S. A. (1994). Late Oligocene-early Miocene unroofing in the Chinese Tien Shan: An early effect of the India-Asia collision. *Geology*, 22(6), 487–490. [https://doi.org/10.1130/0091-7613\(1994\)022<0487:LOEUMI>2.3.CO;2](https://doi.org/10.1130/0091-7613(1994)022<0487:LOEUMI>2.3.CO;2)

- Heubeck, C. (2001). Assembly of central Asia during the middle and late Paleozoic. In Hendrix, M.S., & Davis, G. A. (Eds.), *Paleozoic and Mesozoic Tectonic Evolution of Central Asia: From Continental Assembly to Intracontinental Deformation*: Boulder, Colorado, Geological Society of America Memoir 194, 1–22.
- Hollingsworth, J., Jackson, J., Walker, R., Reza Gheitanchi, M., & Javad Bolourchi, M. (2006). Strike-slip faulting, rotation, and along-strike elongation in the Kopeh Dag mountains, NE Iran. *Geophysical Journal International*, 166(3), 1161–1177. <https://doi.org/10.1111/j.1365-246X.2006.02983.x>
- ISC. (2018). International Seismological Centre, on-line catalogue. <http://www.isc.ac.uk>, International Seismological Centre, Thatcham, UK, last access: 2018-01-25.
- Jackson, J., & McKenzie, D. (1984). Rotational mechanisms of active deformation in Greece and Iran. *Geological Society, London, Special Publications*, 17(1), 743–754. <https://doi.org/10.1144/GSL.SP.1984.017.01.59>
- Jackson, J., McKenzie, D. A. N., Priestley, K., & Emmerson, B. (2008). New views on the structure and rheology of the lithosphere. *Journal of the Geological Society*, 165(2), 453–465. <https://doi.org/10.1144/0016-76492007-109>
- Johnson, K., Nissen, E., Saripalli, S., Arrowsmith, J. R., McGarey, P., Scharer, K., et al. (2014). Rapid mapping of ultrafine fault zone topography with structure from motion. *Geosphere*, 10(5), 969–986. <https://doi.org/10.1130/GES01017.1>
- Jolivet, M., Dominguez, S., Charreau, J., Chen, Y., Li, Y., & Wang, Q. (2010). Mesozoic and Cenozoic tectonic history of the central Chinese Tian Shan: Reactivated tectonic structures and active deformation. *Tectonics*, 29, TC6019. <https://doi.org/10.1029/2010TC002712>
- Kastrup, U., Zoback, M. L., Deichmann, N., Evans, K. F., Giardini, D., & Michael, A. J. (2004). Stress field variations in the Swiss Alps and the northern Alpine foreland derived from inversion of fault plane solutions. *Journal of Geophysical Research*, 109, B01402. <https://doi.org/10.1029/2003JB002550>
- Kober, M., Seib, N., Kley, J., & Voigt, T. (2013). Thick-skinned thrusting in the northern Tien Shan foreland, Kazakhstan: Structural inheritance and polyphase deformation. *Geological Society, London, Special Publications*, 377(1), 19–42. <https://doi.org/10.1144/SP377.7>
- Krüger, F., Kulikova, G., & Landgraf, A. (2015). Instrumental magnitude constraints for the 11 July 1889, Chilik earthquake. *Geological Society, London, Special Publications*, 432(1), 41–72. <https://doi.org/10.1144/SP432.8>
- Kulikova, G., & Krüger, F. (2015). Source process of the 1911 M 8.0 Chon-Kemin earthquake: Investigation results by analogue seismic records. *Geophysical Journal International*, 201(3), 1891–1911. <https://doi.org/10.1093/gji/ggv091>
- Mackenzie, D. (2016). Active shortening in the Alpine-Himalayan belt (PhD thesis). University of Oxford.
- Mackenzie, D., Walker, R., Abdrakhmatov, K., Campbell, G., Carr, A., Grützner, C., et al. (2018). A creeping intracontinental thrust fault: Past and present slip-rates on the northern edge of the Tien Shan, Kazakhstan. *Geophysical Journal International*, 215(2), 1148–1170. <https://doi.org/10.1093/gji/ggy339>
- Maggi, A., Jackson, J. A., McKenzie, D., & Priestley, K. (2000). Earthquake focal depths, effective elastic thickness, and the strength of the continental lithosphere. *Geology*, 28(6), 495–498. [https://doi.org/10.1130/0091-7613\(2000\)28<495:EFDEET>2.0.CO;2](https://doi.org/10.1130/0091-7613(2000)28<495:EFDEET>2.0.CO;2)
- Makarov, V. I. (1977). *New Tectonic Structures of the Central Tien Shan* [in Russian] (p. 171). Moscow: Order of the Red Banner Geology Institute, Akad. Sci.
- Mattei, M., Cifelli, F., Muttoni, G., Zanchi, A., Berra, F., Mossavvari, F., & Eshraghi, S. A. (2012). Neogene block rotation in central Iran: Evidence from paleomagnetic data. *GSA Bulletin*, 124(5–6), 943–956. <https://doi.org/10.1130/B30479.1>
- Molnar, P., Burchfiel, B. C., Ziyun, Z., K'uangyi, L., Shuji, W., & Minmin, H. (1987). Geologic evolution of northern Tibet: Results of an expedition to Ulugh Muztagh. *Science*, 235(4786), 299–305. <https://doi.org/10.1126/science.235.4786.299>
- Molnar, P., & Deng, Q. (1984). Faulting associated with large earthquakes and the average rate of deformation in central and eastern Asia. *Journal of Geophysical Research*, 89(B7), 6203–6227. <https://doi.org/10.1029/JB089iB07p06203>
- Neil, E. A., & Houseman, G. A. (1997). Geodynamics of the Tarim Basin and the Tien Shan in central Asia. *Tectonics*, 16(4), 571–584. <https://doi.org/10.1029/97TC01413>
- Pan, J., Li, H., Sun, Z., Pei, J., Si, J., Barrier, L., et al. (2010). Deformation features of the Mazartagh fold-thrust belt, south central Tarim basin and its tectonic significances. *Dizhi Kexue/Chinese Journal of Geology*, 45(4), 1038–1056.
- Pirajno, F., Mao, J., Zhang, Z., Zhang, Z., & Chai, F. (2008). The association of mafic-ultramafic intrusions and A-type magmatism in the Tien Shan and Altay orogens, NW China: Implications for geodynamic evolution and potential for the discovery of new ore deposits. *Journal of Asian Earth Sciences*, 32(2–4), 165–183. <https://doi.org/10.1016/j.jseaes.2007.10.012>
- Rust, D., Korjenkov, A., & Tibaldi, A. (2018). Geologic slip-rate determinations on the Talas-Fergana fault: Mismatch with geodetic slip rate. *Geophysical Research Letters*, 45, 3880–3888. <https://doi.org/10.1002/2017GL076990>
- Selander, J., Oskin, M., Ormukov, C., & Abdrakhmatov, K. (2012). Inherited strike-slip faults as an origin for basement-cored uplifts: Example of the Kungey and Zailiysky ranges, northern Tien Shan. *Tectonics*, 31, TC4026. <https://doi.org/10.1029/2011TC003002>
- Şengör, A. M. C., Natal'in, B. A., & Burtman, V. S. (1993). Evolution of the Altaid tectonic collage and Palaeozoic crustal growth in Eurasia. *Nature*, 364(6435), 299–307. <https://doi.org/10.1038/364299a0>
- Shean, D. (2017). High Mountain Asia 8-meter DEM Mosaics Derived from Optical Imagery, version 1. Boulder, Colorado USA. NASA National Snow and Ice Data Center Distributed Active Archive Center. doi: <https://doi.org/10.5067/KXOVQ9L172S2> [Accessed on 2017-12-13].
- Sloan, R. A., Jackson, J. A., McKenzie, D., & Priestley, K. (2011). Earthquake depth distributions in central Asia, and their relations with lithosphere thickness, shortening and extension. *Geophysical Journal International*, 185(1), 1–29. <https://doi.org/10.1111/j.1365-246X.2010.04882.x>
- Sobel, E. R., & Dumitru, T. A. (1997). Thrusting and exhumation around the margins of the western Tarim basin during the India-Asia collision. *Journal of Geophysical Research*, 102(B3), 5043–5063. <https://doi.org/10.1029/96JB03267>
- Sobel, E. R., Oskin, M. E., Burbank, D. W., & Mikolaichuk, A. (2006). Exhumation of basement-cored uplifts: Example of the Kyrgyz range quantified with apatite fission-track thermochronology. *Tectonics*, 25, TC2008. <https://doi.org/10.1029/2005TC001809>
- Tatevossian, R. E. (2007). The Verny, 1887, earthquake in central Asia: Application of the INQUA scale, based on coseismic environmental effects. *Quaternary International*, 173–174, 23–29. <https://doi.org/10.1016/j.quaint.2007.02.006>
- Thomas, J. C., Perroud, H., Cobbold, P. R., Bazhenov, M. L., Burtman, V. S., Chauvin, A., & Sadybakasov, E. (1993). A paleomagnetic study of Tertiary formations from the Kyrgyz Tien-Shan and its tectonic implications. *Journal of Geophysical Research*, 98(B6), 9571–9589. <https://doi.org/10.1029/92JB02912>
- Thompson Jobe, J. A., Li, T., Bookhagen, B., Chen, J., & Burbank, D. (2018). Dating growth strata and basin fill by combining ²⁶Al/¹⁰Be burial dating and magnetostratigraphy: Constraining active deformation in the Pamir–Tian Shan convergence zone, NW China. *Lithosphere*, 10(6), 806–828. <https://doi.org/10.1130/L727.1>
- Thompson Jobe, J. A., Li, T., Chen, J., Burbank, D. W., & Bufer, A. (2017). Quaternary tectonic evolution of the Pamir-Tian Shan Convergence Zone, northwest China. *Tectonics*, 36, 2748–2776. <https://doi.org/10.1002/2017TC004541>

- Thompson, S. C., Weldon, R. J., Rubin, C. M., Abdrakhmatov, K., Molnar, P., & Berger, G. W. (2002). Late Quaternary slip rates across the central Tien Shan, Kyrgyzstan, central Asia. *Journal of Geophysical Research*, 107(B9), 2203. <https://doi.org/10.1029/2001JB000596>
- Verestek, V., Appel, E., Voigt, S., & Frisch, K. (2018). Constrained magnetostratigraphic dating of a continental Middle Miocene section in the arid central Asia. *Frontiers in Earth Science*, 6, 49. <https://doi.org/10.3389/feart.2018.00049>
- Voigt, S., Weber, Y., Frisch, K., Bartenstein, A., Hellwig, A., Petschick, R., et al. (2017). Climatically forced moisture supply, sediment flux and pedogenesis in Miocene mudflat deposits of south-east Kazakhstan, central Asia. *The Depositional Record*, 3(2), 209–232. <https://doi.org/10.1002/dep2.34>
- van der Voo, R., Levashova, N. M., Skrinnik, L. I., Kara, T. V., & Bazhenov, M. L. (2006). Late orogenic, large-scale rotations in the Tien Shan and adjacent mobile belts in Kyrgyzstan and Kazakhstan. *Tectonophysics*, 426(3–4), 335–360.
- Walker, R., & Jackson, J. (2004). Active tectonics and late Cenozoic strain distribution in central and eastern Iran. *Tectonics*, 23, TC5010. <https://doi.org/10.1029/2003TC001529>
- Walpersdorf, A., Manighetti, I., Mousavi, Z., Tavakoli, F., Vergnolle, M., Jadidi, A., et al. (2014). Present-day kinematics and fault slip rates in eastern Iran, derived from 11 years of GPS data. *Journal of Geophysical Research: Solid Earth*, 119, 1359–1383. <https://doi.org/10.1002/2013JB010620>
- Wessel, P., & Smith, W. H. (1998). New improved version of Generic Mapping Tools released. *Eos, Transactions of the American Geophysical Union*, 79(47), 579. <https://doi.org/10.1029/98EO00426>
- Westoby, M. J., Brasington, J., Glasser, N. F., Hambrey, M. J., & Reynolds, J. M. (2012). “Structure-from-motion” photogrammetry: A low-cost, effective tool for geoscience applications. *Geomorphology*, 179, 300–314. <https://doi.org/10.1016/j.geomorph.2012.08.021>
- Windley, B. F., Alexeiev, D., Xiao, W., Kröner, A., & Badarch, G. (2007). Tectonic models for accretion of the Central Asian Orogenic Belt. *Journal of the Geological Society*, 164(1), 31–47. <https://doi.org/10.1144/0016-76492006-022>
- Zhang, Z. M., Liou, J. G., & Coleman, R. G. (1984). An outline of the plate tectonics of China. *Geological Society of America Bulletin*, 95(3), 295–312. [https://doi.org/10.1130/0016-7606\(1984\)95<295:AOTPT>2.0.CO;2](https://doi.org/10.1130/0016-7606(1984)95<295:AOTPT>2.0.CO;2)
- Zubovich, A. V., Wang, X., Scherba, Y. G., Schelochkov, G. G., Reilinger, R., Reigber, C., et al. (2010). GPS velocity field for the Tien Shan and surrounding regions. *Tectonics*, 29, TC6014. <https://doi.org/10.1029/2010TC002772>

References From the Supporting Information

- Nelson, M. R., McCaffrey, R., & Molnar, P. (1987). Source parameters for 11 earthquakes in the Tien Shan, central Asia, determined by *P* and SH waveform inversion. *Journal of Geophysical Research*, 92(B12), 12,629–12,648. <https://doi.org/10.1029/JB092iB12p12629>